Using Radiosonde Observations to Assess the "Three Ingredients Method" to Forecast QLCS Mesovortices

MAX D. UNGAR[a,b] AND MICHAEL C. CONIGLIO[c,a]

[a]School of Meteorology, University of Oklahoma, Norman, Oklahoma
[b] Cooperative Institute for Severe and High-Impact Weather Research and Operations, Norman, Oklahoma
[c]NOAA/National Severe Storms Laboratory, Norman, Oklahoma

ABSTRACT: A technique used widely to forecast the potential for QLCS mesovortices is known as the "Three Ingredients Method" (3IM). The 3IM states that mesovortices are favored where 1) the QLCS cold pool and ambient low-level shear are said to be nearly balanced or slightly shear dominant, 2) where the component of the 0–3-km wind shear normal to the convective line is ≥ 30 kt (1 kt ≈ 0.51 m s^{-1}), and 3) where a rear-inflow jet or enhanced outflow causes a surge or bow along the convective line. Despite its widespread use in operational settings, this method has received little evaluation in formal literature. To evaluate the 3IM, radiosonde observations are compared to radar-observed QLCS properties. The distance between the gust front and high reflectivity in the leading convective line (the "U-to-R distance"), the presence of rear-inflow surges, and mesovortices (MVs) were each assessed across 1820 line segments within 50 observed QLCSs. Although 0–3-km line-normal wind shear is statistically different between MV-genesis and null segments, values are ≤ 30 kt for 44% of MV-genesis segments. The 0–6-km line-normal wind shear also shows strong discrimination between MV-genesis and null segments and displays the best linear relationship of the U-to-R distance (a measure of system balance) among layers tested, although the scatter and overlap in distributions suggest that many factors can impact MV genesis (as expected). Overall, most MVs occur where the U-to-R distance lies between -5 and 5 km in the presence of a rear-inflow surge, along with positive 0–1-km wind shear, 0–3-km wind shear > 10 kt, and 0–6-km wind shear > 20 kt (all line-normal).

SIGNIFICANCE STATEMENT: Near the leading edge of thunderstorm lines, areas of rotation that can produce tornadoes and strong winds ("mesovortices") often develop rapidly. Despite advances in understanding mesovortices, few operational guidelines exist to anticipate their genesis. One popular method used to forecast mesovortices—the "Three Ingredients Method"—is evaluated in this study. Our work confirms the importance of two of the ingredients—a surge of outflow winds and thunderstorms that stay nearly atop the leading edge of the outflow. However, we find that many mesovortices occur below the threshold of low-level wind shear ascribed by the forecast method. Refinements to the method are suggested, including the favorable distance between the leading edge of the outflow and thunderstorm updrafts and lower bounds of wind shear over multiple layers, below which mesovortices may be unlikely.

1. Introduction

Quasi-linear convective systems (QLCSs) often pose a risk to life and property through the generation of mesovortices (MVs) that can produce damaging straight-line winds and tornadoes (Atkins et al. 2005; Wakimoto et al. 2006; Wheatley et al. 2006). Approximately 20% of tornadoes across the central and eastern United States may be attributable to QLCSs (Trapp et al. 2005; Ashley et al. 2019). While most QLCS MV tornadoes are weak—rated a 0 or 1 on the (enhanced) Fujita (EF) scale—strong/intense QLCS tornadoes do occur (Trapp et al. 2005; Smith et al. 2012). Beyond the presence of severe convective hazards, MVs can develop quickly, relative to our ability to routinely observe them, presenting a challenge in current warning decision-making. Brotzge et al. (2013) and Gibbs and Bowers

(2019) note that QLCS tornadoes have a lower probability of detection (POD), a higher false alarm rate (FAR), and a greater number of "missed events" for significant (EF2+) tornadoes than their supercell counterparts.

Understanding the mechanisms behind the generation of QLCS MVs has been the topic of many studies over the past two decades. Common to most of these studies is the presence of a convectively generated cold pool of air that is crucial to the development and maintenance of the parent QLCS (Hane 1973; Thorpe et al. 1982; Rotunno et al. 1988). However, the degree to which cold pool properties are important can be modulated by large-scale forcing mechanisms, particularly when conditional instability is relatively weak (van den Broeke et al. 2005; Jewett and Wilhelmson 2006; Evans 2010; King et al. 2017). Idealized simulations have shown that MV genesis can occur by the tilting and subsequent stretching of baroclinic horizontal vorticity generated by the cold pool within updrafts (Atkins and St. Laurent 2009a,b) or downdrafts (Weisman and Trapp 2003; Trapp and Weisman 2003; Wakimoto et al. 2015). Other mechanisms that can contribute to MV genesis, and that are less dependent on cold-pool baroclinicity, include the release of horizontal shearing

---

Corresponding author: Max D. Ungar, max.ungar@noaa.gov

instability (HSI) (Carbone 1983; Lee and Wilhelmson 1997a,b; Wheatley and Trapp 2008; Conrad and Knupp 2019; Goodnight et al. 2022) and the tilting and stretching of frictionally induced horizontal vorticity (Schenkman et al. 2012, 2014; Xu et al. 2015). Recent studies note that MV-genesis mechanisms may be quite varied, even within the same QLCS (Lovell and Parker 2022). Processes like those that generate low-level rotation in supercells, including the downward tilting of horizontal vorticity associated with descending rear-inflow jets (RIJs) (Atkins and St. Laurent 2009a,b; Wakimoto et al. 2015; Flournoy and Coniglio 2019) and possibly the ingestion of large low-level horizontal streamwise vorticity (Schenkman et al. 2014; Flournoy and Coniglio 2019), may also generate MVs in QLCSs.

Despite growing knowledge of MV-genesis mechanisms, a relative lack of predictive tools currently exists in operational settings to assist forecasters in anticipating MV genesis. One attempt to address this need is the "Three Ingredients Method" (henceforth 3IM), developed by Schaumann and Przybylinski (2012) (henceforth SP12). The 3IM defines favored QLCS MV-genesis conditions to help in their early prediction and warning and can be summarized as follows:

1) a portion of a QLCS in which the system cold pool and ambient low-level shear are nearly balanced or slightly shear dominant;
2) where 0–3-km line-normal bulk shear magnitudes are ≥30 kt (1 kt ≈ 0.51 m s^{-1}); and
3) where an RIJ or enhanced outflow causes a surge or bow in the line.

The first ingredient describes the relationship between ambient environmental vertical wind shear and the system cold pool. Although there are different interpretations of *why* this relationship is important for squall lines (Xu and Moncrieff 1994; Bryan and Rotunno 2014; Alfaro 2017; Alfaro and Lezana 2022), this ingredient invokes the principles described in Rotunno et al. (1988) who show, in simplified conditions, that a certain amount of low-level shear is needed to balance the vorticity generated by the cold pool to maximize lifting of environmental air (Rotunno et al. 1988; Weisman and Rotunno 2004; Bryan and Rotunno 2014). Without ambient low-level shear (i.e., horizontal vorticity), vorticity generated by the cold pool sweeps inflowing air rearward, and updrafts are subsequently weaker than if they were more vertical (Parker 2010). Likewise, inflowing parcels within strong shear regimes (i.e., shear dominant modes) lean in the downshear direction and tend to be weaker than their balanced counterparts (assuming they are not supercellular).

Although the concepts mentioned above are derived in two dimensions under several dynamical constraints, the importance of ambient shear in approximately the same layer occupied by the cold pool to produce deep lifting is also observed in less-constrained squall-line simulations across various models and levels of realism (Weisman et al. 1988; Bryan et al. 2006; Bryan and Rotunno 2014; Mulholland et al. 2021). Aside from the cold pool/shear effects on overall QLCS behavior, Atkins and St. Laurent (2009a,b) show that deep and nearly upright updrafts along the gust front facilitates the most efficient stretching of near-surface vertical vorticity, which is an important component to MV genesis.

While some amount of low-level shear is vital to counter the detrimental effects of the cold pool on upright updrafts in simplified conditions, studies attempting to apply these results to real-world squall lines have suggested that additional factors can promote nearly balanced systems (Stensrud et al. 2005). Shear induced by rear-inflow jets within the cold pool (Weisman et al. 1992) and shear above the cold pool can bring systems closer to a balanced state and increase lifting (Shapiro 1992; Szeto and Cho 1994; Fovell and Dailey 1995; Coniglio et al. 2006), particularly when low-level shear is suboptimal in the Rotunno et al. (1988) framework. One consequence of shear above the cold pool is the so-called "updraft in shear" effect (Parker and Johnson 2004); as updrafts ascend through shear above the cold pool, a pressure-perturbation gradient develops that promotes updraft propagation in the downshear direction leading to updrafts closer to the leading edge of the cold pool. When shear extends above the cold pool, Coniglio et al. (2006) show that parcels rise for longer periods above the gust front and can produce deeper lifting than would otherwise occur if shear was weaker and confined to low levels. A motivation for exploring this latter result is that shear is often observed to extend well above cold pools in QLCS environments (Thompson et al. 2012). Cohen et al. (2007) and Coniglio et al. (2006) highlighted the greater utility in using deep-layer shear to quantify the overall severity and maintenance of QLCSs compared to shear over shallower depths.

Other studies (James et al. 2005; Alfaro 2017; Mulholland et al. 2021) emphasize that differences in low-level mass flux and the modulating effects of low-level shear on entrainment in updrafts can have a strong control on QLCS behavior. These factors may be particularly important when cold pools are deep and lifting becomes "slabular" meaning lifting occurs in layers rather than solely in individual convective cells locally along the gust front, the latter of which may be more applicable to the vorticity-balance perspective of Rotunno et al. (1988). However, regardless of the physics at play, it is apparent that balanced QLCSs become more favored as the shear increases, and a nearly balanced system may be crucial for the development of MVs through strong updrafts persisting close to the gust front.

The second ingredient of the 3IM is achieved when the magnitude of the environmental wind shear in the lowest 3 km above ground level[1] normal to the convective line is ≥30 kt. SP12 notes (based on examining wind shear computed from unspecified model output) that the likelihood of MVs increases as the 0–3-km line-normal wind shear passes this threshold. In general, a line-normal wind shear of 30 kt (~15 m s^{-1}) is also consistent with the idealized experiments of Trapp and Weisman (2003) who identified 20 m s^{-1} of wind shear in the 0–2.5-km layer to favor the presence of cyclonic MVs within QLCSs. Concurrently, Atkins and St. Laurent (2009a) note weaker and shorter-lived MVs tend to develop when wind shear is <15 m s^{-1} in 0–2.5- and 0–5-km layers (although cold pool strengths in these studies were not varied). Later studies that explore MV-genesis

_____

[1] Henceforth, all references to heights refer to above ground level.

mechanisms typically use shear profiles well above this threshold (Marion and Trapp 2021; Lovell and Parker 2022).

SP12 notes that the physical significance of the 30-kt threshold is unclear, although it is assumed to be tied to the vorticity-balance principles of Rotunno et al. (1988), which are derived in a two-dimensional plane normal to the cold pool. Therefore, it is the *line-normal component* of the shear that is beneficial for a balanced state. Additionally, the findings of Engerer et al. (2008), who used cold pool pressure rises from Oklahoma Mesonet observations as a proxy for assessing cold pool strength/depth across hundreds of mesoscale convective systems, were interpreted by SP12 to imply that 15 m s^{-1} (30 kt) of low-level shear is strong enough to balance a "typical" cold pool. It should be noted that the Engerer et al. (2008) findings use a regionally confined set of observations, and thus, applying them across regionally disparate environments may come with caveats. Clearly, the first and second 3IM ingredients are physically connected in the sense that QLCSs capable of MV genesis are assumed to have cold pools where a moderate amount of opposing shear is needed to produce vertically upright updrafts of sufficient strength to support MVs. The choice of 30 kt by SP12 partially reflects this concept, but it could also be important as a source of horizontal vorticity to be tilted into the vertical (Trapp and Weisman 2003; Atkins and St. Laurent 2009a,b; Wakimoto et al. 2015).

The third ingredient of the 3IM is the presence of a surge or bow within the main convective line, caused by an RIJ or enhanced outflow. The RIJ in QLCSs has been extensively studied since the mid-twentieth century, with Fujita (1978) describing the damage potential of the descending RIJ at the bowing apex or leading edge of the surge. Additional studies (Jorgensen and Smull 1993; Przybylinski 1995; Atkins et al. 2004; Wakimoto et al. 2015) have further validated early findings and have shown that surface wind damage can often be traced to the presence of a mesoscale RIJ. Atkins et al. (2004) also noted that all tornadic vortices observed within a QLCS during the Bow Echo and MCV Experiment (BAMEX) field campaign formed coincident with the genesis of an RIJ. The above studies focus on the impacts of mesoscale RIJs, but later studies show that smaller-scale surges, related to enhanced downdrafts or embedded microbursts, may be associated with MV genesis (Atkins and St. Laurent 2009b; Newman and Heinselman 2012; Xu et al. 2015; Flournoy and Coniglio 2019).

The physical importance of an RIJ surge to MV genesis is not entirely known, but one direct possibility is the abundance of cyclonic shear along the gust front and on the north side of surges that can break down (through HSI) into vortices and subsequently stretched into MV strength (Carbone 1982; Conrad and Knupp 2019). Wakimoto et al. (2006), Atkins and St. Laurent (2009b), and Flournoy and Coniglio (2019) show that horizontal vorticity, generated baroclinically along localized downdrafts/surges, can be tilted downward to generate cyclonic vertical vorticity that is then stretched to MV strength. Localized surges may also act to help tilt inflowing crosswise environmental vorticity on the south side of the surge into cyclonic vertical vorticity on the north side (Flournoy and Coniglio 2019).

To evaluate the 3IM, and to concurrently explore environmental controls on QLCS MV-genesis potential, this study

assesses both internal QLCS properties and environmental characteristics in relation to 50 observed QLCSs. WSR-88D observations are used to assess the internal system properties including the relative shear/cold pool balance of each system (ingredient 1), RIJ features and localized outflow surges (ingredient 3), and the presence of MVs. Radiosonde observations (soundings) from both field programs and operations[2] (National Weather Service) are used to evaluate the 30-kt 0–3-km line-normal shear threshold (ingredient 2), as well as the impact of varying shear magnitudes and depths for MV-genesis outcomes.

The primary goals of this study are to evaluate the 3IM, to identify scenarios where the 3IM may not properly identify QLCS MV genesis, and to develop operational recommendations in these scenarios. To the authors' knowledge, this study represents one of the few to quantitatively test the 3IM approach over a large dataset of observed cases. Of note, Gibbs (2021) assessed the 3IM, along with combinations of environmental MV-genesis precursors outlined by National Weather Service (NWS) Warning Decision Training Division (WDTD) guidance, to assess its skill in identifying MV-genesis tornado environments. The 3IM was found to demonstrate reasonable skill for QLCS tornado prediction, especially when combined with additional environmental variables. The discussion herein differs from Gibbs (2021) in a few fundamental ways. First, this study attempts to objectively quantify the shear/cold pool balance regime observed with each QLCS with the method described in section 2. Additionally, the assessment of wind shear from *observed* proximity soundings, along with different wind shear depths and orientations, is novel to this study.

2. Data and analysis methods

a. Case selection overview

To quantitatively assess the performance of the 3IM, a dataset of QLCS events, spanning the period from 1 January 2010 through 31 December 2020, was constructed. This included data from multiple field experiments, including Plains Elevated Convection At Night (PECAN; Geerts et al. 2017) and the various NOAA-sponsored Verification of the Origins of Rotation in Tornadoes Experiment-Southeast (VORTEX-Southeast; Rasmussen et al. 2015) campaigns. All convective periods (1200–1200 UTC), spanning the above period, within the Storm Prediction Center Storm Events Database that have at least one severe wind or tornado report were also included for preliminary analysis.

Composite (column-maximum) radar reflectivity imagery was interrogated for all identified convective periods to determine primary storm mode using the Interactive National Reflectivity

---

[2] Data from the field-project soundings were accessed via the Earth Observing Laboratory (EOL) (available at https://www.eol.ucar.edu/all-field-programs), and data for the National Weather Service soundings were accessed via the National Center for Environmental Information (NCEI) Integrated Global Radiosonde Archive (IGRA) version 2 (available at https://www.ncei.noaa.gov/pub/data/igra). WSR-88D data were accessed via NCEI/Amazon Cloud Database (available at https://s3.amazonaws.com/noaa-nexrad-level2/index.html).
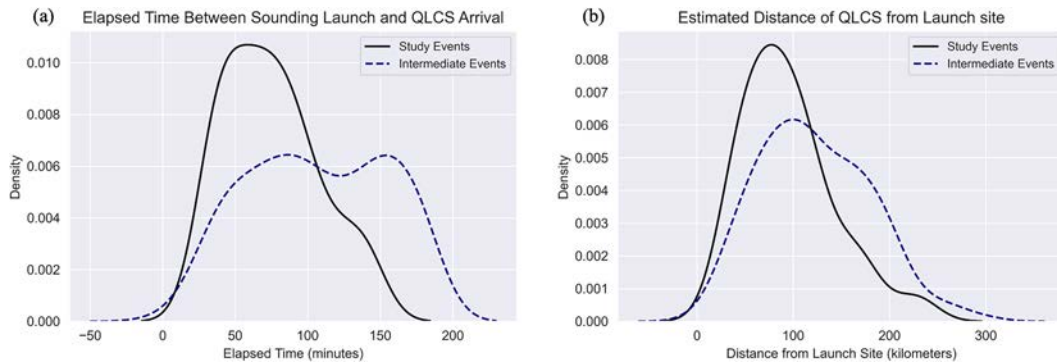
FIG. 1. Kernel density estimation (KDE) plots of (a) elapsed time (min) between sounding release and QLCS arrival at release location and (b) shortest distance (km) between the QLCS and the sounding release location at release time comparing the 50 selected study events (black) to "intermediate events" (dashed blue).

Mosaic from the National Centers for Environmental Information (NCEI; available at https://www.ncei.noaa.gov/maps/radar/). While many criteria to define a QLCS exist in the literature, this study follows the definition used by Haberlie and Ashley (2019) of a contiguous or semicontiguous line (≥100 km) of convective cores (≥40 dBZ) that persists at least three hours. Applying these criteria, and using the NCEI interactive mosaic, over 500 QLCSs were identified in the study period.

To expedite the case selection process, and ensure omission of cases with long spatiotemporal lag to the relevant sounding profiles, QLCSs were not considered in this analysis if there was no sounding released ≤3 h and/or ≤200 km on their inflow side. In addition, omitting soundings that likely sampled unrepresentative environments (e.g., post-convective releases, those that contained superadiabatic lapse rates or wet-bulb temperature profiles from heavy precipitation) reduced the number of potential QLCSs to 125 [18 field program/107 operational (NWS)] tied with 208 proximity soundings. The remaining 125 QLCSs ("intermediate events") were further interrogated using WSR-88D Level-II data using the Gibson Ridge 2 Analyst (GR2Analyst) version 2.80 software. This additional case refinement was done to identify QLCSs that 1) best maintained QLCS structure (based on Haberlie and Ashley 2019) while approaching the sounding release location and 2) were closest in space/time to the sounding release. For the former, we retained those QLCSs that best resembled a "classic" QLCS structure of a contiguous linear region of high reflectivity. In practice, it is often difficult to confidently prescribe a single convective mode to linear-type convection, as embedded supercells or highly 3D structures sometimes evolve rapidly within linear-type systems (Smith et al. 2012; Ashley et al. 2019). The more complex QLCS structures, with some evidence of "discreteness" (i.e., cellular structures/ updrafts with gaps in requisite (>40 dBZ) reflectivity), were avoided here in favor of the more clearly linear structures. In total, 50 QLCSs were selected for analysis.[3] The majority

(~80%) of study cases arrived within 2 h of the sounding release with a mean QLCS distance of ~95 km from the release location (Figs. 1 and 2). Additionally, nearly three-quarters (76%) of selected cases met an acceptable criterion for a "1-hour" proximity profile (i.e., temporal lag between 30 and 90 min to feature of interest). This is akin to Thompson et al. (2003), and related later studies, who chose the closest analysis grid hour to time of severe report for their definition of a proximity profile. Additionally, nearly half of QLCSs (~44%) arrived ≤1 h from the proximity sounding release. When considering the study case with longest temporal lag (i.e., proximity sounding release until QLCS arrival), tested variables (section 2) are comparable in the ~2 h between sounding release (~2300 UTC) and the last analysis available prior to the QLCS arrival, as estimated by the Storm Prediction Center objective mesoanalysis (Fig. 3). Finally, magnitudes of tested kinematic variables (sections 3b and 3d) from observed soundings in this study were compared against vertical wind profile (VWP) hodographs (when available, 44 of 50 cases). VWP hodographs from the closest/ collocated WSR-88D radar, at time nearest to sounding release, were assessed here. Comparisons across all wind shear depths evaluated (section 3) show little separation among the two observational techniques, with each failing to show statistically significant differences when applying a Student's t test (not shown) (Fig. 4). Despite the limitations in using proximity sounding data (discussed further in section 4), the above discussion, and comparisons to other observational techniques, offers support to the outcomes discussed herein. Additionally, the regional dispersion of cases (Fig. 5) matches well with previous QLCS climatological studies (Smith et al. 2012; Ashley et al. 2019), most notably with the highest density of QLCSs across the Mississippi, Ohio, and Missouri River valleys. The climatological similarity to past studies extends to the seasonality of study events (Fig. 6), with ~60% of the QLCSs occurring between April and July.

b. Radar analysis

Only those portions of a QLCS within 100 km from the radar site, and within the final hour prior to the QLCS arrival at the sounding release site, were analyzed via WSR-88D data. Best resolution of assessed MV and gust front characteristics

---

[3] The time-intensive nature of the analysis method described later led to stopping the analysis at 50 cases.
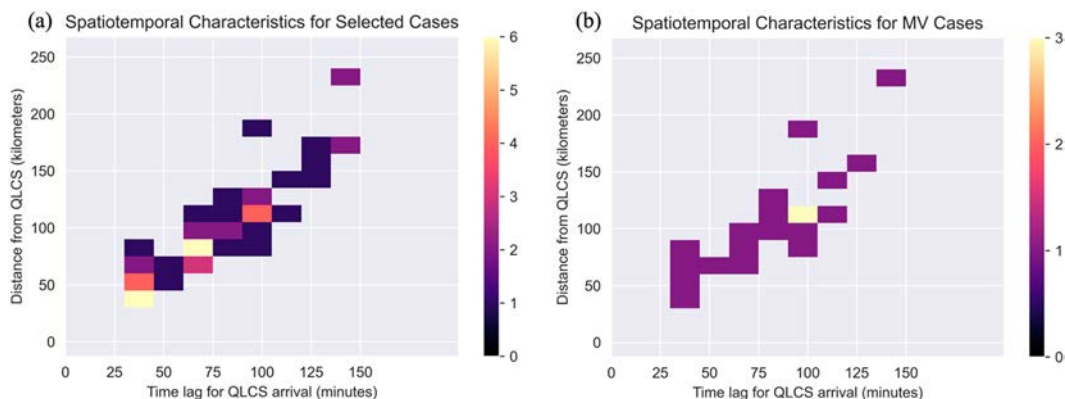
FIG. 2. Tile plots displaying the spatiotemporal characteristics of (a) all study (50) cases and (b) cases containing at least one MV-genesis event (21). Warmer colors represent a greater number of cases according to the color bar.

[sections 2b(1) and 2b(4)] occurs at smaller distances from a single site radar. Because of the manual, labor-intensive nature of the radar analysis, every other *full* volume scan within the previously described range of time and distance constraints was examined, which resulted in analyses every 10–12 min.

1) ASSESSMENT OF INGREDIENT 1: SHEAR/COLD POOL BALANCE

As discussed previously, the first ingredient (henceforth ingredient 1) of the 3IM attempts to assess the relative balance between the cold pool and ambient environmental shear. However, this condition is difficult to quantify in practice because the cold pool depth and the vertical distribution of buoyancy are required and cannot be estimated accurately using routine observations. This facilitates the need to approximate ingredient 1 via alternate approaches. The approach used in SP12 and in this study is to assume a system is balanced, with nearly upright convection, when high radar reflectivity is located close to the leading edge of the cold pool/gust front. Likewise, a gust front that has surged well ahead of the strongest convection within the line is assumed to represent an upshear-tilted (cold-pool dominant) system, and one with updrafts tilted away from the cold pool represents a downshear-tilted (shear dominant) system. This is based on the bevy of past QLCS simulations that generally show cold-pool dominant convection to slant upshear along the gust front (either individual updrafts or in a time-mean sense), placing the strongest convective cores and reflectivity behind the gust in radar imagery. The opposite effect (from a radar imagery perspective) occurs for shear dominant systems.

In practice, the gust front, or as defined by SP12, the updraft–downdraft convergence zone (UDCZ), can be identified following Schaumann and Gagan (2018) using a four-panel radar visualization (illustrated in Figs. 7 and 8). Broadly speaking, the UDCZ can be identified where sharp gradients in spectrum width and velocity (magnitudes) exist. Distance between the UDCZ and high reflectivity within the convective line was used to approximate the balanced state of the QLCS.[4] Given uncertainties in the exact position of the convective line, the UDCZ-to-reflectivity (U-to-R) distance was computed for three reflectivity values (40, 45, and 50 dBZ), along with an "All" dBZ distance (the mean of the 40-, 45-, and 50-dBZ distances). Because QLCS properties can vary in the along-line dimension, the above steps were repeated (beginning from the first point meeting the QLCS criteria on the northernmost portion of the line) every 15 km along the convective line until the next analysis point fell ≥100 km from the radar, the convective line (≥40-dBZ echoes) reached the sounding release location, and/or no echoes ≥ 40 dBZ were assessed. An overview of this process is shown in Fig. 9. The final U-to-R distances used in the analysis are averages of two adjacent calculation points, resulting in U-to-R distances every 15 km along the line. For example, in Fig. 9, the U-to-R distances at points A and B (representing analysis points along the analyzed UDCZ) are averaged to compute a mean U-to-R distance representative of the along-line region between A and B, likewise for points B and C, and continuing down the line. While variability in the U-to-R distance can occur over spatial scales smaller than 15 km, this approach captures at least some of the mesoscale along-line variability of the QLCS orientation and U-to-R distances while also balancing against the overall time burden of this manual approach. In total, 1820 line segments (each 15 km in length) were analyzed among the 50 studied QLCSs.

Occasionally, convective cells or "enhanced stratiform" reflectivity (>40 dBZ) occurred immediately ahead of the main UDCZ that complicated the calculation of the U-to-R distance. Figures 9 and 10 illustrate examples in which leading-line convective cores and "enhanced stratiform" reflectivity

---

[4] Single- and dual-polarimetric products can have small time discrepancies, which were accounted for when computing the U-to-R distances through manual interpolation of the position of the features. The position of the UDCZ was primarily assessed using spectrum width and storm-relative velocity/motion. In the GR2Analyst software, these products have a slightly longer processing time lag when compared to reflectivity imagery over each volume scan.
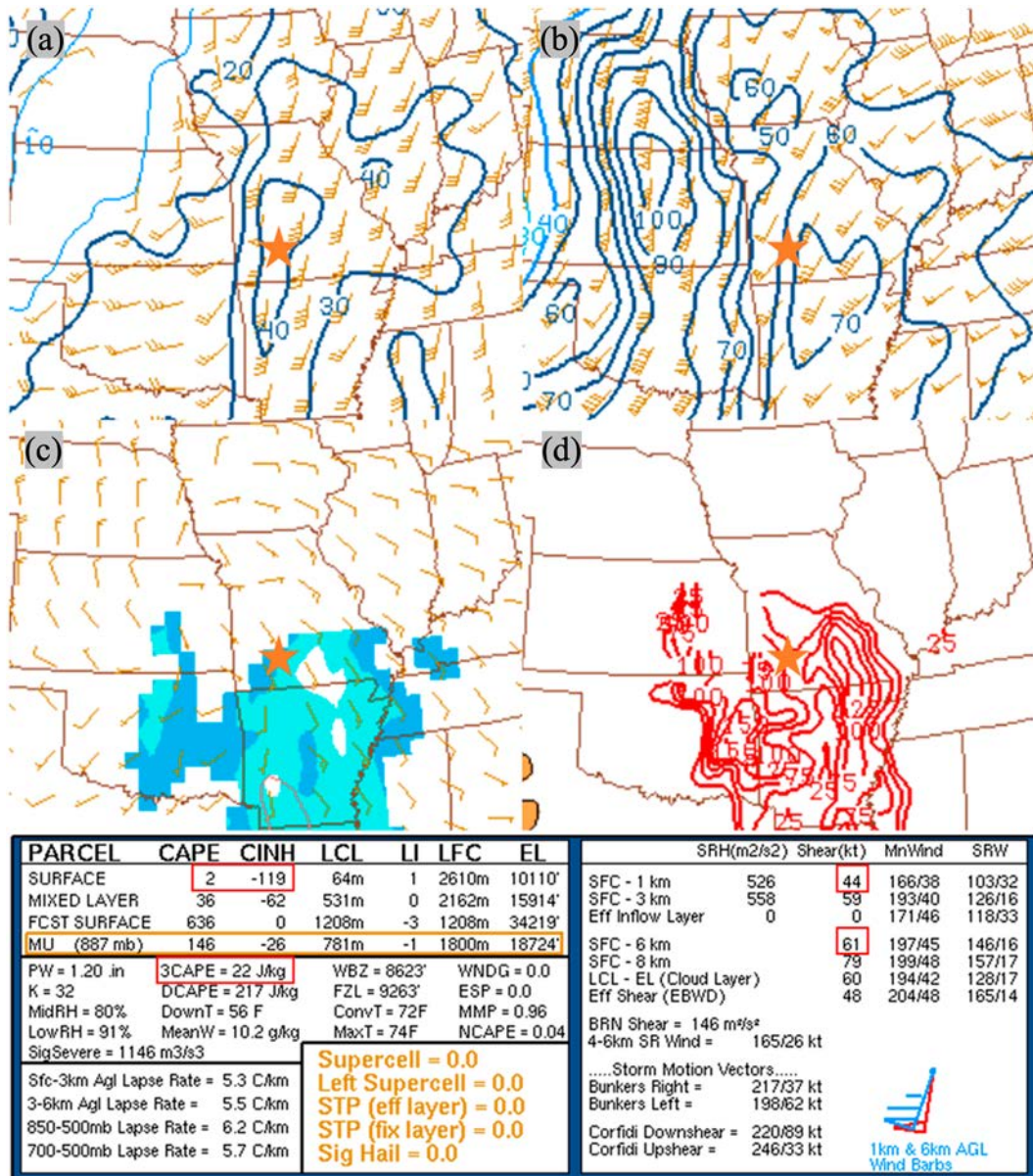
PARCEL	CAPE	CINH	LCL	LI	LFC	EL
SURFACE	2	-119	64m	1	2610m	10110'
MIXED LAYER	36	-62	531m	0	2162m	15914'
FCST SURFACE	636	0	1208m	-3	1208m	34219'
MU (887 mb)	146	-26	781m	-1	1800m	18724'

PW = 1.20 .in	3CAPE = 22 J/kg	WBZ = 8623'	WNDG = 0.0
K = 32	DCAPE = 217 J/kg	FZL = 9263'	ESP = 0.0
MidRH = 80%	DownT = 56 F	ConvT = 72F	MMP = 0.96
LowRH = 91%	MeanW = 10.2 g/kg	MaxT = 74F	NCAPE = 0.04
SigSevere = 1146 m3/s3			

Sfc-3km Agl Lapse Rate = 5.3 C/km	Supercell = 0.0
3-6km Agl Lapse Rate = 5.5 C/km	Left Supercell = 0.0
850-500mb Lapse Rate = 6.2 C/km	STP (eff layer) = 0.0
700-500mb Lapse Rate = 5.7 C/km	STP (fix layer) = 0.0
	Sig Hail = 0.0

	SRH(m2/s2)	Shear(kt)	MnWind	SRW
SFC - 1 km	526	44	166/38	103/32
SFC - 3 km	558	59	193/40	126/16
Eff Inflow Layer	0	0	171/46	118/33
SFC - 6 km		61	197/45	146/16
SFC - 8 km		79	199/48	157/17
LCL - EL (Cloud Layer)		60	194/42	128/17
Eff Shear (EBWD)		48	204/48	165/14

BRN Shear = 146 m²/s²
4-6km SR Wind = 165/26 kt

.....Storm Motion Vectors.....
Bunkers Right = 217/37 kt
Bunkers Left = 198/62 kt

Corfidi Downshear = 220/89 kt
Corfidi Upshear = 246/33 kt

1km & 6km AGL Wind Barbs

FIG. 3. Storm Prediction Center objective mesoscale analysis valid at 0100 UTC 29 Dec 2019. (a) 0–1-km wind shear vectors (barbs) and magnitude (contours). (b) As in (a), but over the 0–6-km depth. (c) Surface-based convective available potential energy (CAPE) (contours), 10-m winds (barbs), and convective inhibition (CIN; shaded). (d) Mixed-layer CAPE within the 0–3-km depth (red contours). (bottom) An overview of observed measures from the 0000 UTC sounding launch from National Weather Service, Springfield, MO. The orange star represents the approximate location of the National Weather Service, Springfield, MO, upper-air release site. Images courtesy of the NOAA Storm Prediction Center Severe Event Archive.

were deemed distinct enough from the QLCS to compute U-to-R distances using only the 50-dBZ threshold, as using lower dBZ thresholds created ambiguity regarding convection that was tied to the UDCZ/gust front. In total, 561 out of the 1820 segments are missing at least one (i.e., 40, 45, and/or 50 dBZ) measure because of this ambiguity. Removing an additional 25 segments that contain no U-to-R distance measurement (primarily due to beam blockage), the number of

segments in the final analysis containing all four U-to-R distance measures computed is 1234.

2) ASSESSMENT OF INGREDIENT 2: 0–3-KM LINE-NORMAL SHEAR

The second ingredient (henceforth ingredient 2) of 3IM is 0–3-km line-normal wind shear, assessed from the proximity
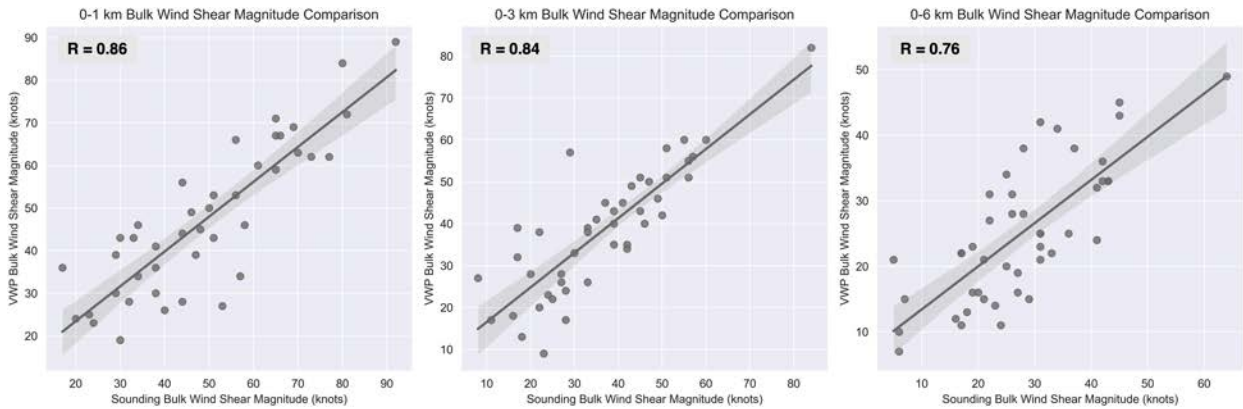
FIG. 4. (left) Scatterplot comparison of 0–1-km bulk wind shear as analyzed from vertical wind profile hodographs (VWP) vs sounding profiles. A linear regression line is represented as the gray line (95% confidence interval, via bootstrapping) with the Pearson correlation coefficient (R) displayed in the top-left corner. (center) As in the left panel, but for a comparison of 0–3-km bulk wind shear. (right) As in the left panel, but for a comparison of 0–6-km bulk wind shear.

sounding associated with each QLCS case. The 0–3-km wind shear (henceforth 3Shear) was computed by a simple subtraction of the 10-m wind vector from the (linearly interpolated) 3-km wind vector. An online tool/GUI (Pennsylvania State Univ.; https://courseware.e-education.psu.edu/courses/meteo361/javascript/Lesson3/shear_calc.html), along with manual calculation applying the Law of Cosines, helped determine the

appropriate 3Shear vector from the individual (surface and interpolated 3 km) wind components. To compute the component of the 3Shear normal to the convective line, the initial bearing between the latitude/longitude of adjacent analysis points (e.g., A and B in Fig. 9) was used to define the line segment orientations, which were then compared against the 3Shear vector. A similar process is shown in
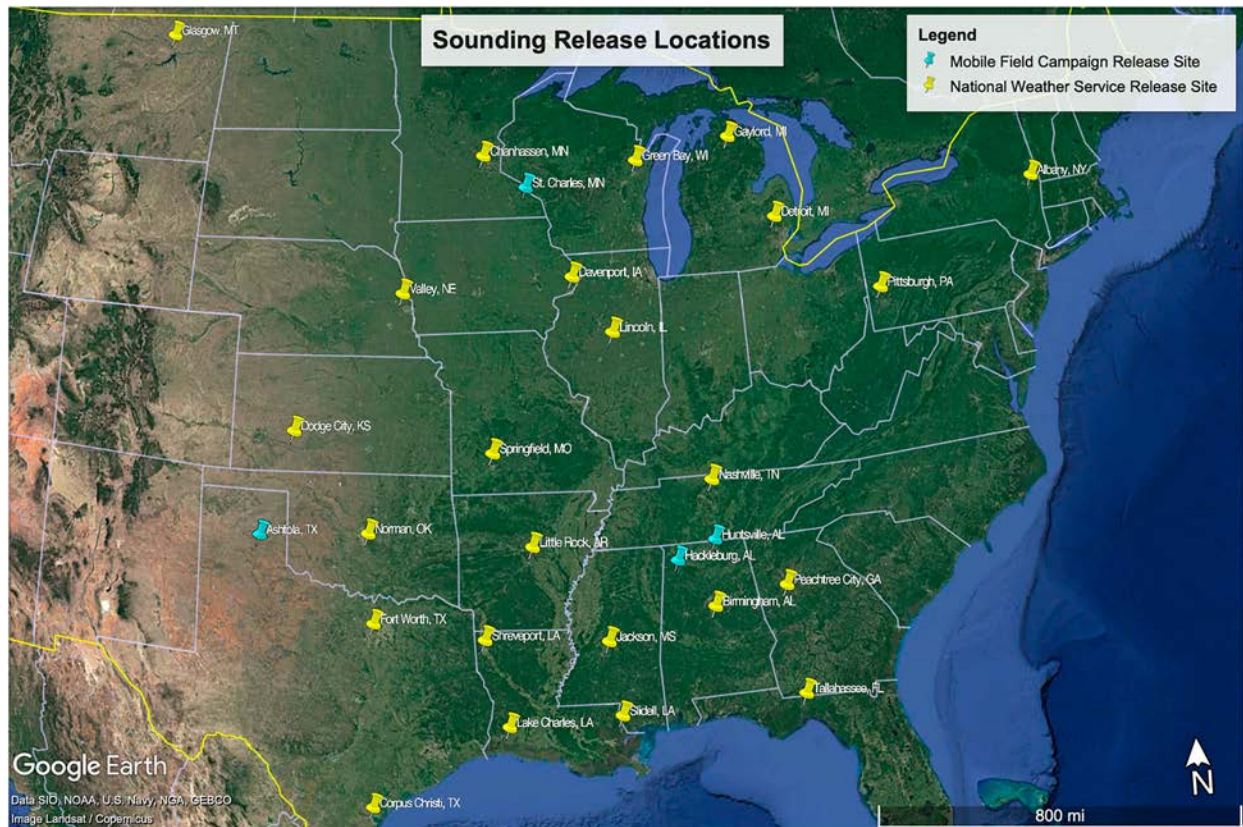
FIG. 5. Geographical overview of proximity sounding release sites. Image created using Google Earth software.
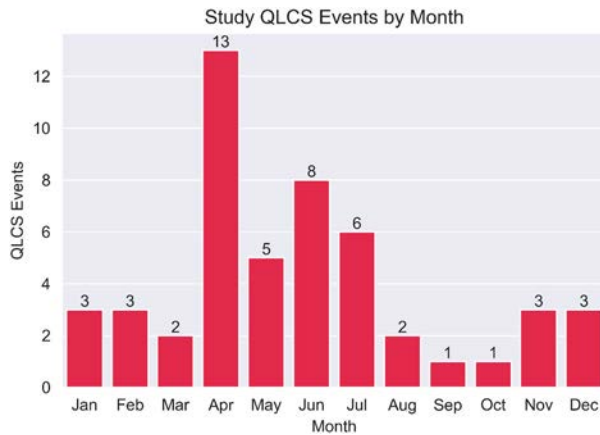
FIG. 6. Bar graph plot showing distribution, by month, of 50 study QLCS cases.

Fig. 11. A magnitude of line-normal 3Shear was then computed for all 1820 unique line segments among the 50 studied QLCSs.

3) ASSESSMENT OF INGREDIENT 3: REAR-INFLOW SURGES

The third ingredient (henceforth ingredient 3) of the 3IM assesses surges or bows within the convective line, often induced by an RIJ or enhanced outflow. Identification of rear-inflow surges was conducted manually by (visually) comparing the character of radial flow relative to the reflectivity structure

of the UDCZ (Fig. 12). A surge was noted to occur across any segment where an otherwise "straight" (meridional) UDCZ was perturbed, or in other words, displayed a bowing structure (in radar imagery). In general, bows (surges), the size as those displayed in Fig. 12, and smaller, were considered in this analysis.

4) RADAR ASSESSMENT OF MESOVORTICES

Following SP12 and operational practices (J. Schaumann 2022, personal communication), an area of storm-scale rotation, identified in storm-relative velocity/motion, was considered an MV if

1) rotational velocities (VROTs) $\geq$ 20 kt;
2) the VROT criterion was met at every scan below 8000 ft ($\sim$2438 m); and
3) persisted at least two full volume scans.

Previous studies have applied similar approaches to identify MVs via WSR-88D data interrogation (Smith et al. 2015; Sessa and Trapp 2020). Qualitatively, these criteria follow the findings of Atkins et al. (2004), which describe tornadic MVs as being "longer-lived and stronger at low levels" and deepening rapidly prior to tornadogenesis. In applying the above criteria, 42 unique MVs (*within 39 unique line segments*) across 21 of the 50 QLCSs were identified. Because the focus of the 3IM is on conditions that support the genesis of MVs, we explore differences in distributions between these 39 line segments for which an MV developed ("MV-genesis segments") and the remaining segments with no MVs ("null segments").
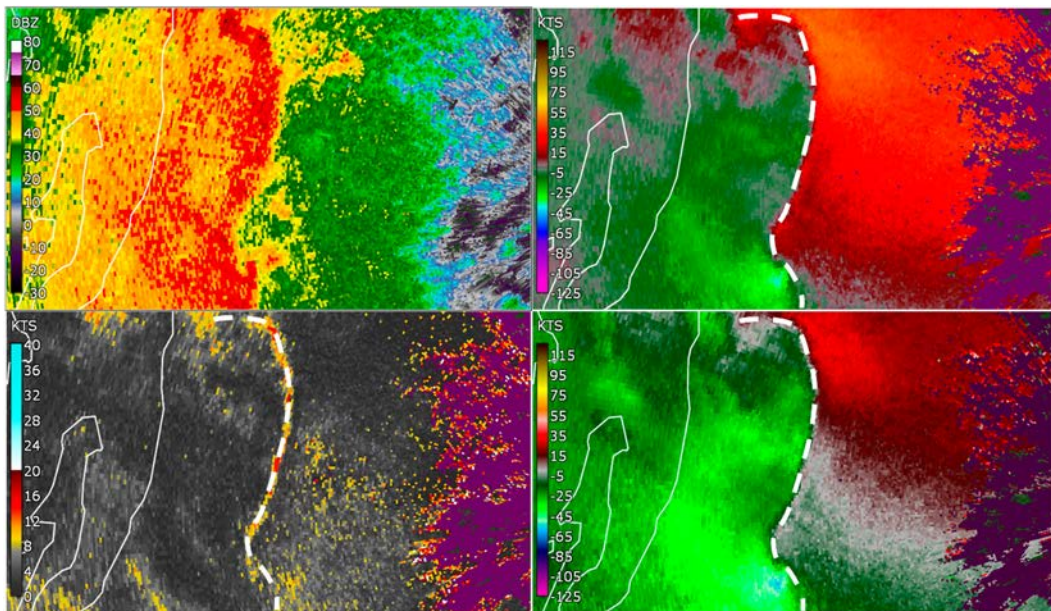
FIG. 7. Four-panel visualization in Gibson Ridge 2 Analyst (GR2Analyst) for assessing U-to-R distance (i.e., shear/cold pool balance) as shown in Schaumann and Gagan (2018). (from top left and moving clockwise) Radar reflectivity (dBZ), storm-relative velocity/motion (SRV/M), base velocity (BV), and spectrum width (SW). Image from Gaylord, MI (KAPX), (at 0.5° elevation) valid at 2304 UTC 28 Aug 2018. The dashed white line represents an approximation of UDCZ position at 2304 UTC in a typical manner to that conducted at each analysis period.
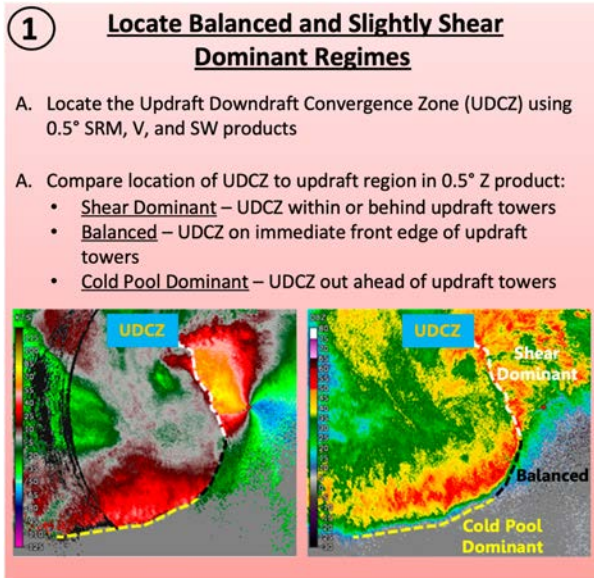
FIG. 8. Overview of study-adjacent methodology of how to analyze and determine the balance state of a QLCS. Obtained from a graphic produced by the National Weather Service Central Region Convective Warning Improvement Project (CR-CWIP) team.

During the radar analysis of MVs, multiple areas of rotation often occurred that failed to meet one of the above MV conditions. These weaker/shorter-lived signatures, for which one MV criterion is not met, are termed "transient mesovortices" (MVTs). In total, 47 unique MVTs (within 47 unique line segments) were identified across 27 of the 50 QLCSs.

The focus of this study is evaluating the original "Three Ingredients Method"; however, we also explore differences in

distributions for different wind shear orientations and depths guided by the MV and QLCS process studies mentioned in the introduction (section 1). Furthermore, given the large disparity between MV and null segments (~1:32 ratio), we evaluated MV outcomes relative to operational guidance (WDTD/CR-CWIP QLCS "nudgers"; Fig. 13) intended to raise forecaster situational awareness to a *tornadic* MV threat. This included a particular focus on low-level (0–3-km) instability, although two additional (non-"nudger") thermodynamic variables (0–1-km lapse rate and LCL height), hypothesized to favor *tornadic* outcomes, were also evaluated (Thompson et al. 2003; Kirkpatrick et al. 2007; Sherburn and Parker 2014). Preliminary outcomes show that LCL height (of a mixed-layer parcel) *may* prove useful in differentiating tornadic versus nontornadic MV signatures. However, even so, with nearly half of tornadic cases occurring after local sunset time, results may show temporal skew. With only 9 MVs associated with a confirmed tornado in this dataset, thermodynamic outcomes are not presented here and await the development of a larger dataset of cases/MVs. Additionally, no substantial differences among the thermodynamic variables tested were identified between MV-genesis segments and null segments. Therefore, only kinematic variables related to ingredients 1 and 2, and their impact to MV genesis, are discussed further.

3. 3IM evaluation results

a. Ingredient 1: 3Shear/cold pool balance

As discussed previously, ingredients 1 and 2 are not independent. Ingredient 1, or a cold pool in a balanced or slightly shear dominant regime, is theorized to be favored when ingredient 2, or the line-normal 3Shear, is ≥30 kt. Therefore, a direct comparison of the first two ingredients can help illustrate the relative strength of this theorized relationship. In
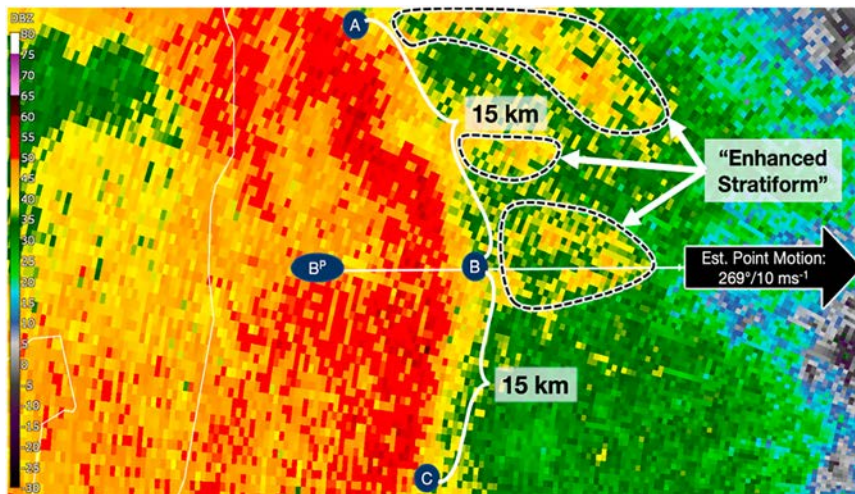

FIG. 9. A portion of a study QLCS across northern Michigan on 28 Aug 2018. Image from KAPX (at 0.5° elevation) valid at 2325 UTC. Point "B^P" represents position of point "B" (analysis point) at the prior analysis period (i.e., full volume scan), which is used to determine the storm motion vector and the path along which U-to-R distances are computed. Points "A" and "C" represent additional analysis points in the along-line direction at 15-km intervals.
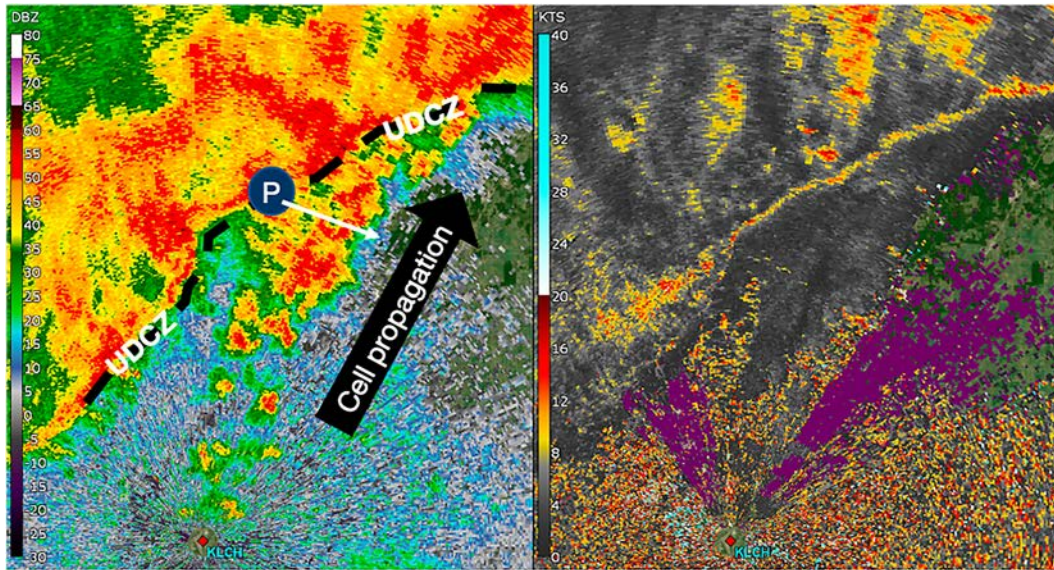
FIG. 10. A portion of a study QLCS across southwest Louisiana on 4 Apr 2014. Image from Lake Charles, LA (KLCH), (at 0.5° elevation) valid at 1217 UTC. (left) Radar reflectivity and (right) spectrum width. The dashed black line represents the identified position of UDCZ. Point "P" and the white arrow represent a plausible analysis location and U-to-R calculation path, respectively.

other words, comparing ingredients 1 and 2 provides observational evidence of how much the balanced state (estimated by the U-to-R distance herein) relates to the ambient line-normal shear.
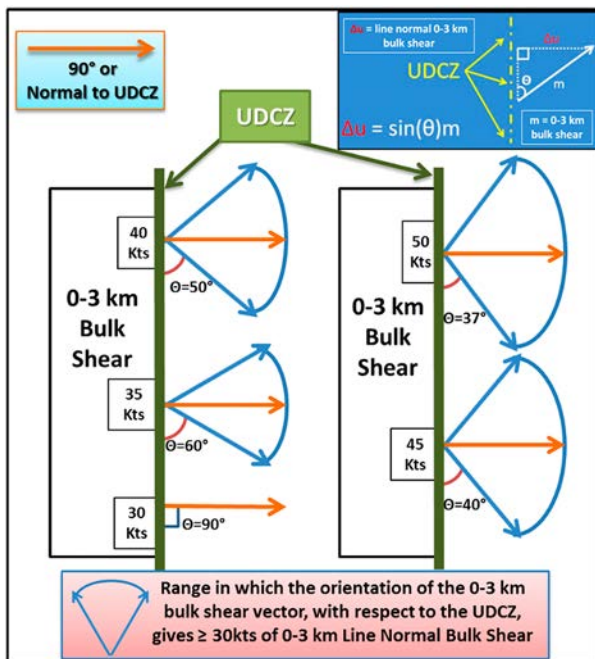
FIG. 11. Methodology to determine the line-normal component of wind shear used in this study and in operational settings. Obtained from a graphic produced by the National Weather Service CR-CWIP team.

First, the U-to-R distances for the 1626 line segments that contain a valid 50-dBZ distance were compared to the line-normal 3Shear (Fig. 14). The 50-dBZ threshold is used to illustrate the relationship between ingredients because all MV-genesis segments are captured using this value as discussed earlier [section 2b(1)]. Overall, a weak-to-moderate negative linear relationship is evident between these two variables (Pearson correlation coefficient, or R, of -0.27). As line-normal 3Shear increases from small values, the U-to-R distance tends to decrease toward zero or negative values (i.e., the convective line becomes closer aligned, or leans away from, the gust front) as expected. However, only 7% of the variance in the U-to-R distance is explained by the line-normal 3Shear (R^2 magnitude of 0.07), indicating that the U-to-R distance is likely influenced by additional factors. Figure 14 also shows that ~79% (31/39) of MV-genesis segments (red dots) have a U-to-R distance between -4 and 4 km (using the 50-dBZ threshold). Physically, this means that updraft cores (centroid of highest analyzed radar reflectivity when calculating the U-to-R distance) are between 4 km behind and 4 km ahead of the UDCZ for ~79% of MV-genesis events. This percentage increases to ~90% if the range is extended to ± 5 km. This agrees with the assessment in SP12 that portions of QLCSs that tend to produce MVs are usually nearly balanced or slightly shear dominant (at least to the degree that the U-to-R distance can be used as a proxy for the degree of balance of the system).

Additional comparisons were made to assess ingredients 1 and 2 using the 40- and 45-dBZ thresholds among the 1403 and 1392 individual segments, respectively. While not shown, none of these comparisons result in substantial differences and continue to yield weak-to-moderate (negative) linear correlation
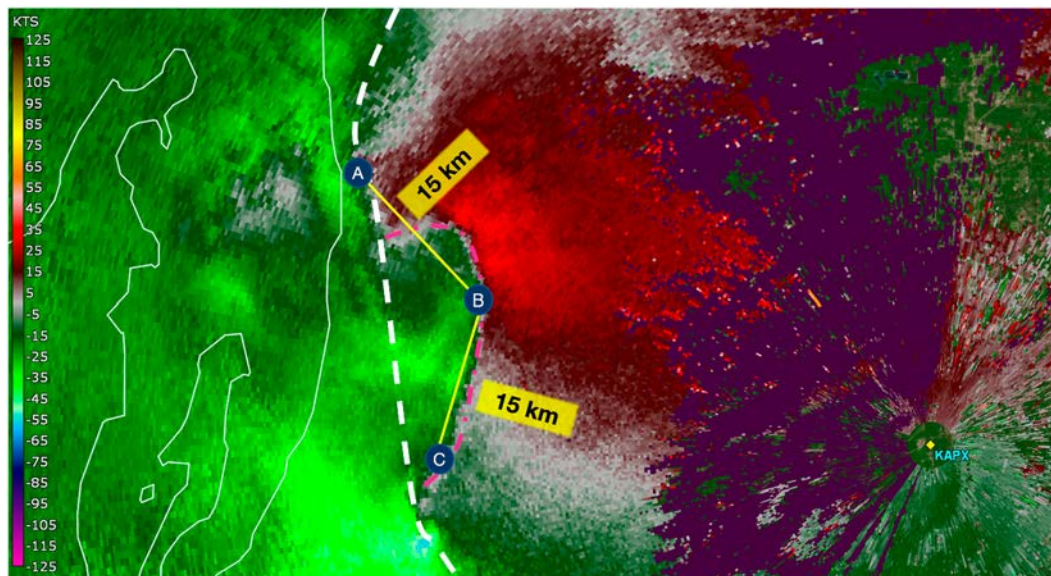
FIG. 12. Example of the process to determine rear-inflow/outflow surges. Base velocity (BV) image (at 0.5° elevation) from KAPX valid at 2316 UTC 28 Aug 2018. Positions "A," "B," and "C" represent U-to-R analysis positions. The yellow line represents the "AB" and "BC" line segments (15 km in length). The dashed white line represents a hypothetical (locally) meridional UDCZ displaying no perturbations in flow structure. The dashed–dotted magenta line represents the outline of an identified surge.

$(−0.27 > R > −0.34)$ as with using the 50-dBZ threshold. MV-genesis segments, across all additional reflectivity thresholds, continue to observe U-to-R distances mostly between $−5$ and 5 km.

b. Ingredient 2: Distribution of bulk and line-normal 0–3-km wind shear

The distribution of *bulk* 3Shear magnitudes among the 50 QLCSs is approximately normal, with a peak near 30 kt (Fig. 15). Among all 1820 line segments, the peak in the distribution of the *line-normal* 3Shear is ~18 kt (Fig. 15). When only considering the 39 line segments associated with MV genesis, the peak in the distribution is only slightly larger (~21 kt), which reveals that many MV-genesis events (17 out of 39, or ~44%) occurred with line-normal 3Shear under the 3IM threshold value.

Although many events occur with line-normal 3Shear under 30 kt, the line-normal 3Shear does tend to be larger for MV-genesis segments than for null segments (Fig. 16a). However, a significant overlap still exists between these distributions (e.g., the 25th–50th percentile of MV-genesis segments and the 50th–70th percentile of null segments). Furthermore, the mean and median of the line-normal 3Shear for MV-genesis segments are ~30 kt. For transient MVs (MVT-genesis segments), not only is the mean and median of the line-normal 3Shear < 30 kt, there is even greater overlap of the distributions between segment outcomes (Fig. 16b). This has important ramifications on the utility of ingredient 2 as a means to identify favorable MV-genesis segments. *If one intends to use the line-normal 3Shear as a true lower threshold below which QLCS MVs become unlikely, then* Figs. 15 *and* 16 *suggest that a substantially smaller value than*

30 kt may be more appropriate. While study cases are widely spaced across the continental United States (CONUS), especially east of the Rocky Mountains, the requisite shear threshold may also show seasonal and/or temporal variance and should be investigated in future studies.

c. Ingredient 3: Presence of rear-inflow surges

As shown in Fig. 17a, a momentum surge in the convective line is present for a large majority of MV-genesis segments (33 out of 39, or 85%). This agrees with SP12, along with numerous other observational and numerical studies, on the importance of this feature for MV genesis. A fewer proportion of MVT-genesis segments are associated with surges (28/47, or 60%; Fig. 17b).

d. Additional shear depths and orientations

Additional interrogation of the QLCS environments was performed by exploring other shear depths and orientations relative to the convective line. First, the results of Flournoy and Coniglio (2019) were used as motivation to explore the relationship of the low-level line-*parallel* wind shear to MV genesis. Flournoy and Coniglio (2019) analyzed trajectories of parcels that populated a mesovortex within a real-data simulation of a PECAN QLCS. One source of cyclonic vertical vorticity in the mesovortex (at levels above ~500 m) was low-level (100–300 m AGL) inflow parcels from the ambient environment within very strong near-ground vertical wind shear oriented *parallel* to the gust front. As air flowed toward the QLCS at a small angle to the convective line, the crosswise horizontal vorticity within the environment was tilted into the vertical on the south side of a local outflow surge which contributed to cyclonic vertical vorticity on the north side of the surge. Given this finding, and the common occurrence
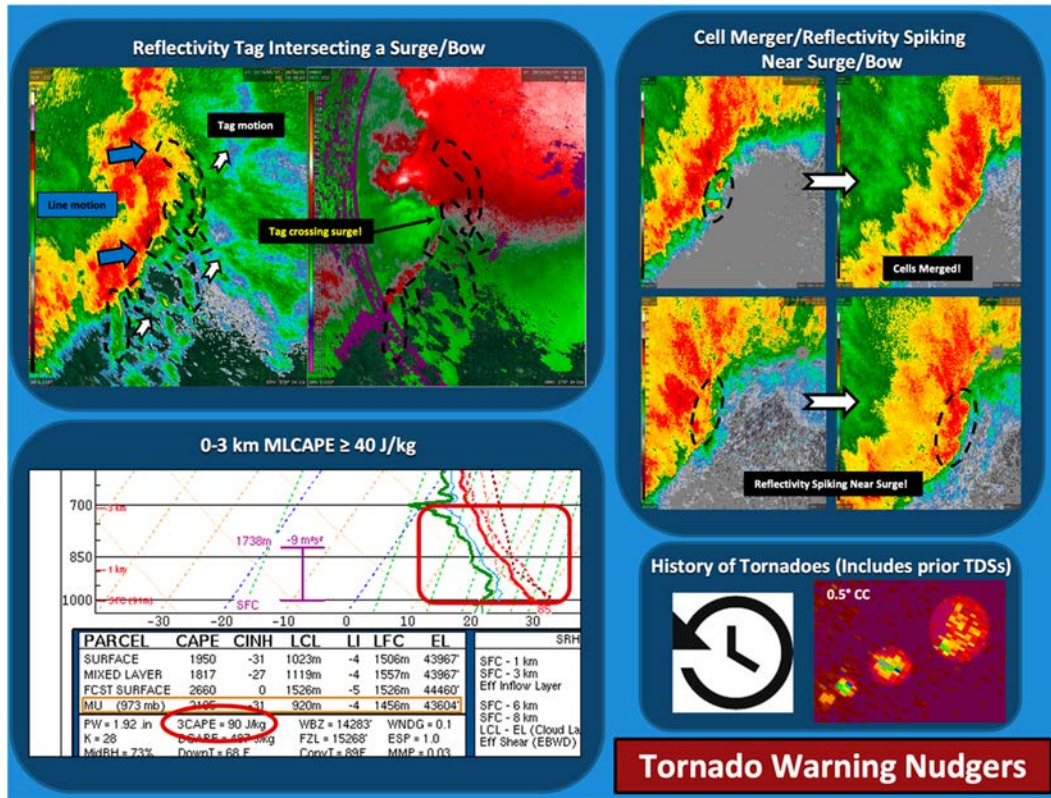
FIG. 13. Infographic from the Warning Decision Training Division (WDTD) and National Weather Service CR-CWIP team outlining "nudgers," used as warning precursor signatures, when applying the 3IM in operational settings.

of strong, meridional low-level jets in ~north–south-oriented QLCS environments, we first assessed whether 0–1-km wind shear (henceforth 1Shear) in the line-*parallel* direction showed utility in discriminating MV-genesis potential. Additionally, in

FIG. 14. Scatterplot comparing the U-to-R distance to line-normal 0–3-km wind shear using the 50-dBZ reflectivity threshold (positive indicating a gust front ahead of main convective cores). A linear regression line is represented as the gray line (95% confidence interval, via bootstrapping, shown as light gray shading), with the Pearson correlation coefficient (R) displayed in the top-left corner. Red scatters represent segments where MV genesis was assessed.

line with the original 3IM approach, the line-normal component of shear in the lowest 1 km was also explored given that cold pools may be shallower than 3 km, especially across the southeastern United States where buoyancy is often limited in the cool season (Sherburn and Parker 2014).

First, for line-normal 1Shear (Fig. 18), the linear relationship to the U-to-R distance is even weaker than it is for the line-normal 3Shear (R of −0.22 for the former compared to −0.27 for the latter). Furthermore, the magnitude of line-normal 1Shear is a slightly weaker discriminator than line-normal 3Shear for MV-genesis events (not shown). For line-*parallel* 1Shear, there is little to no linear relationship to the U-to-R distance as expected (Fig. 19). There is no clear physical reason to expect this relationship for line-parallel shear as opposed to line-normal shear, but the results are presented this way for continuity with the other figures. Figure 19 also shows no evidence that the distributions of line-parallel 1Shear are different for MV-genesis segments compared to null segments. Finally, we ask the question, does line-parallel 1Shear tend to be large when the line-normal 3Shear is relatively small for MV-genesis cases in the dataset? In other words, does the MV-genesis process favored in strong low-level line-parallel shear described in Flournoy and Coniglio (2019) compensate for weaker line-normal 3Shear? The answer appears to be *no*, as there is a weak positive relationship between line-parallel 1Shear and line-normal 3Shear (Fig. 20). This latter result does not mean that the processes inherent in strong line-parallel shear described in Flournoy and Coniglio (2019) did not occur in
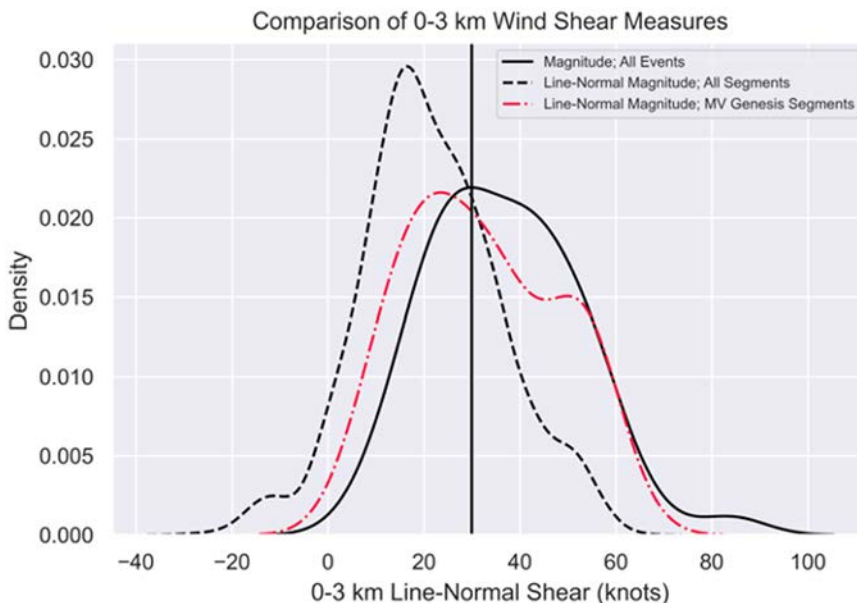
FIG. 15. Kernel density estimation distribution comparison of 0–3-km bulk wind shear magnitude among the 50 QLCS soundings (solid black line), line-normal 0–3-km wind shear among the 1820 line segments (dashed black line), and line-normal 0–3-km wind shear associated with the 39 MV-genesis line segments (dashed–dotted red line). The vertical black line delineates the 30-kt threshold of the 3IM.

our cases; rather, this simply suggests that these processes do not appear to have been the common way that MVs developed in the cases with weak line-normal 3Shear.

Focusing on the MV-genesis segments in Figs. 18 and 19, a few additional takeaways are evident. Most notably, a large proportion of MV-genesis segments occurred with 0–20 kt of line-normal 1Shear and 10–30 kt of line-parallel 1Shear. More generally, 0 kt of line-normal and 10 kt of line-parallel 1Shear are reasonable lower bounds for MV-genesis segments in the study dataset. This suggests that MVs require at least some

positive line-normal low-level shear (oriented rear-to-front relative to the orientation of the gust front). Likewise, the bottom threshold of 10 kt for line-parallel shear might be used as a lower limit for when MVs can be expected. However, this may simply reflect that QLCSs tend to occur in environments of enhanced low-level southerly flow in the convectively unstable warm sector of approaching larger-scale cyclones, and may not indicate any routine storm-scale dynamical importance of the line-parallel shear for MV genesis.
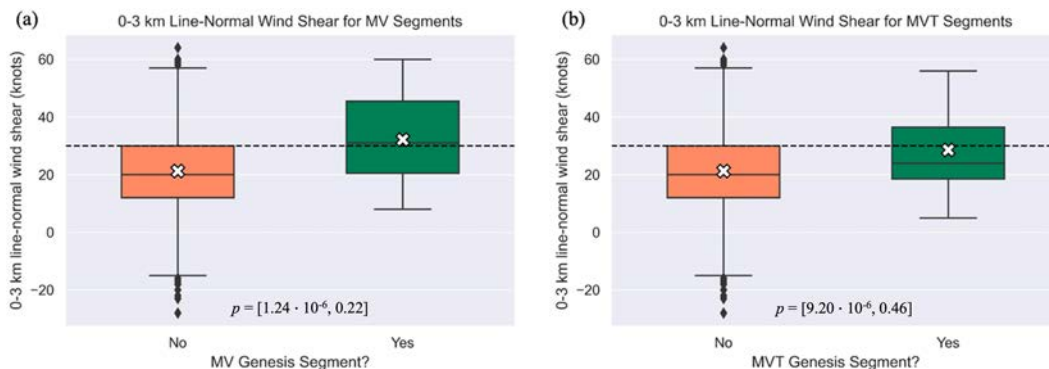

FIG. 16. (a) Boxplot of line-normal 0–3-km wind shear comparing MV-genesis (green) and null (orange) segments. (b) As in (a), but now assessing segments that observed "transient" (MVT)-genesis (green). The black-dashed line delineates the 30-kt threshold of the 3IM. Boxes cover the IQR (25th–75th percentiles), and whiskers extend to the 10th and 90th percentiles, with outlier values in the null cases indicated as diamonds. Calculated p values, with an effective sample size of $n = 39$ in (a) and $n = 47$ in (b), are displayed at the bottom center of each panel. Values indicate the inner 95% distribution of p values obtained via bootstrapping.
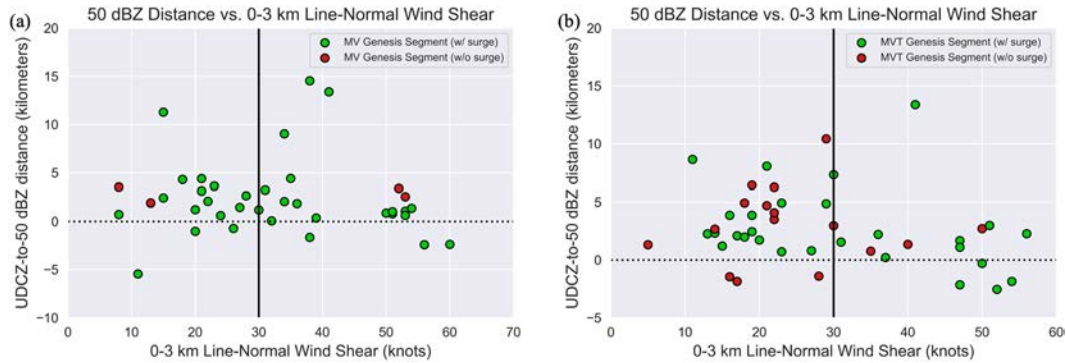
FIG. 17. Scatterplot of ingredients 1 and 2, using the 50-dBZ threshold U-to-R distance for (a) all MV-genesis segments and (b) MVT-genesis segments. The vertical black line represents the 30-kt wind shear threshold. Coloring represents subdivision based on MV-genesis and surge occurrences (green = surge present and dark red = no surge present).

The impact of using 0–6-km wind shear (henceforth 6Shear) was assessed based on the studies discussed previously suggesting better discriminatory ability of deep-layer wind shear compared to low-level wind shear for the severity and longevity of QLCSs (Cohen et al. 2007; Coniglio et al. 2007). While the overall (negative) linear relationship remains modest, *the best linear relationships between (all) U-to-R distance radar reflectivity thresholds and line-normal shear are seen when using 6Shear* (−0.42 < R < −0.33). Figure 21, capturing the 6Shear relation when using the 50-dBZ threshold, displays an R value of −0.33, although relationships using lower reflectivity thresholds (i.e., 40/45 dBZ) displayed the highest R values of any comparison (−0.42, not shown). Radar ambiguity issues [discussed in section 2b(1)] reduced the sample size of MV segments when using the 40- and 45-dBZ measures, and so the relationship for the 50-dBZ threshold is shown to maximize the sample size. *This*

suggests that line-normal 6Shear best relates (linearly) to the balanced state of the system rather than the line-normal 3Shear and 1Shear, although the substantial scatter continues to show that other factors can control the U-to-R distance (the balance state) of the QLCS. In terms of discriminating MV-genesis segments against null segments, line-normal 6Shear shows a significant *visual* separation of interquartile ranges (like that of line-normal 3Shear), with the mean and median of MV-genesis segments lying above the 75th percentile for null segments (Figs. 16a and 22). Line-normal 3Shear shows a slightly stronger signal of *statistical* significance compared to line-normal 6Shear based on distributions of bootstrapped p values (bottom center of Figs. 16a and 22). However, as discussed above, given similar distributions (and interquartile ranges) between line-normal 3Shear and 6Shear, we note similar *practical* application of each shear depth in our dataset.
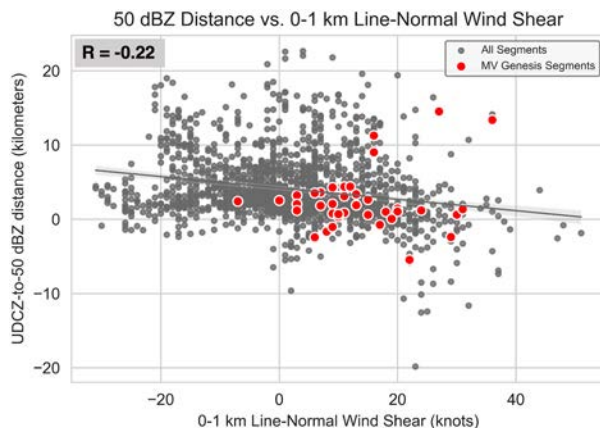

FIG. 18. Scatterplot comparing the U-to-R distance to line-normal 0–1-km wind shear using the 50-dBZ reflectivity threshold. A linear regression line is represented as the gray line (95% confidence interval, via bootstrapping, shown as light gray shading), with the Pearson correlation coefficient value (R) displayed in the top-left corner. Red scatters represent segments where MV genesis was assessed.
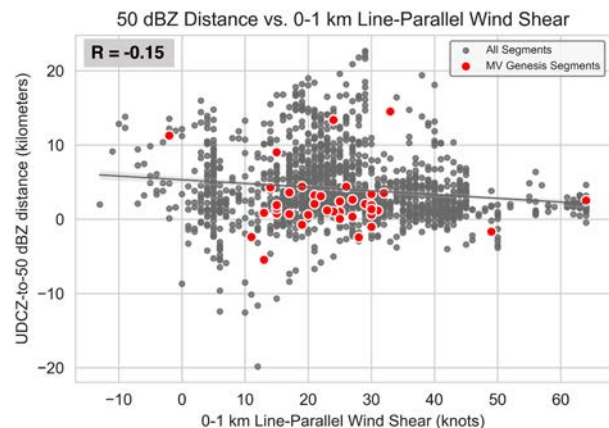
FIG. 19. Scatterplot comparing the U-to-R distance to line-parallel 0–1-km wind shear using the 50-dBZ reflectivity threshold. A linear regression line is represented as the gray line (95% confidence interval, via bootstrapping, shown as light gray shading), with the Pearson correlation coefficient value (R) displayed in the top-left corner. Red scatters represent segments where MV genesis was assessed.

Comparing 0–1 km Line-Parallel vs. 0–3 km Line-Normal Shear for MV Genesis
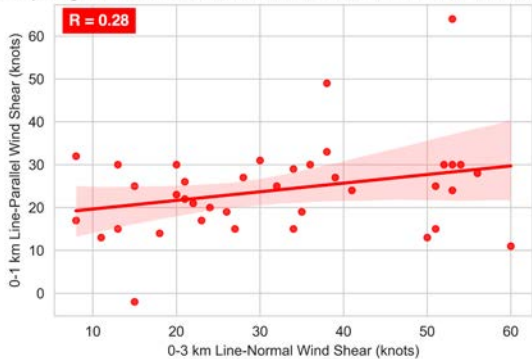

FIG. 20. Scatterplot comparing 0–1-km line-parallel vs 0–3-km line-normal wind shear over MV-genesis line segments. The linear regression line represented as the red line (95% confidence interval, via bootstrapping, shown as light red shading), with the Pearson correlation coefficient value (R) displayed in the top-left corner.

4. Summary and conclusions

Discussion

This study explored 50 quasi-linear convective systems (QLCSs) to evaluate the "Three Ingredients Method" (3IM) for forecasting QLCS mesovortices (MVs). Developed by Schaumann and Przybylinski (2012), the 3IM was designed to incorporate both internal and external QLCS characteristics to aid in early identification of MVs. The first ingredient of the 3IM is met when ambient environmental shear and the system cold pool are said to be balanced or slightly shear dominant. The shear/cold pool balance of each system was estimated by measuring the distance between the updraft–downdraft convergence zone (UDCZ) and three reflectivity (dBZ) thresholds (termed the "U-to-R distance") every 15 km along the convective line. The second 3IM ingredient is line-normal wind shear magnitudes, in the bottom 3 km of the atmosphere, of at least 30 kt. This magnitude of line-normal 0–3-km wind shear (3Shear) is hypothesized to promote a favorable shear/cold pool balance regime. Wind shear magnitudes were assessed using radiosonde observations taken in proximity to each study QLCS. The line-normal shear was assessed across 15-km line segments over a roughly 1-h period of analysis (concurrent with U-to-R distance calculation) for each of the 50 QLCSs (1820 in total). The third 3IM ingredient is the presence of a bow or surge of the main convective line, generally resulting from enhanced outflow or rear-to-front flow. A subjective radar analysis was employed to determine the presence of rear-inflow surges among the study cases.

A key finding was that almost half of the MV-genesis events are observed with line-normal 3Shear below the 3IM threshold (30 kt). In addition, line-normal shear within the 0–3-km layer showed only a modest linear relationship against the U-to-R distance. There are likely many reasons for these two results, relating to the general likelihood that more factors than line-normal 3Shear and the relative cold pool strength control the generation of MVs and the degree of balance within a QLCS.
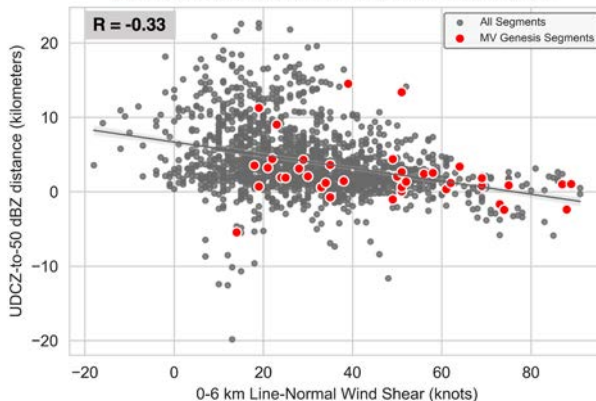
50 dBZ Distance vs. 0–6 km Line-Normal Wind Shear

FIG. 21. Scatterplot comparing the U-to-R distance to line-normal 0–6-km wind shear using the 50-dBZ reflectivity threshold. A linear regression line is represented as the gray line (95% confidence interval, via bootstrapping, shown as light gray shading), with the Pearson correlation coefficient value (R) displayed in the top-left corner. Red scatters represent MV-genesis segments.

Investigating wind shear over additional layers and orientations revealed that statistical discrimination between MV/MVT and null segments is strongest when applying line-normal wind shear in the 0–3-km layer as ascribed by SP12 (as seen by bootstrapped p-value distributions in Figs. 16a and 22). Conversely, line-normal 0–6-km shear, not 0–3-km wind shear, provided the strongest relationship to the U-to-R distance ($R = -0.42$ versus -0.27 using the 40-dBZ threshold, not shown). This indicates a greater ability to distinguish potential storm structure and small U-to-R distance more so than shallower shear depths. This result agrees with past studies (Cohen et al. 2007; Coniglio et al. 2007) that show the best discrimination between the severity and longevity of QLCSs is provided when using deep-layer shear variables. However, aforementioned

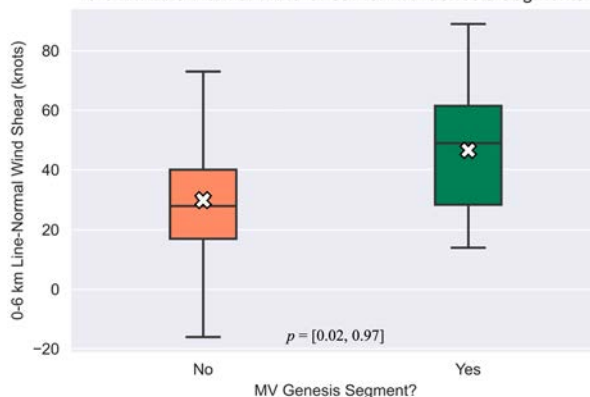0–6 km Line-Normal Wind Shear for MV Genesis Segments

FIG. 22. As in Fig. 16, but for line-normal 0–6-km wind shear binned by MV-genesis outcome. Calculated p values, with an effective sample size of $n = 39$, are displayed in the bottom center. Values indicate the inner 95% distribution of p values obtained via bootstrapping.

linear relationships are modest and combined with substantial overlap in shear distributions (Figs. 16a and 22) suggest that multiple factors beyond those examined in this study control both MV-genesis and overall QLCS structure.

Also noteworthy is that almost all MV-genesis segments occurred with line-normal 6Shear > 20 kt. This is an interesting outcome because a wind profile with low-to-mid-level shear largely parallel to the convective line can still be favorable for linear/QLCS modes (Dial et al. 2010). Indeed, 29% of the total line segments documented here occurred with 6Shear < ~20 kt. Parker and Johnson (2004) show that QLCSs with weak line-normal and strong line-parallel deep-layer shear often orient themselves in a parallel stratiform configuration. Our analysis suggests that MV genesis is *not* favored in these types of QLCSs and that some deep-layer shear oriented line-normal is important in MV genesis (as one of the multiple favorable environmental factors).

The importance of deep-layer shear likely links to the parent QLCS structure more so than to the development of the MVs themselves. To explore reasons for why many MVs still occurred in relatively weak line-normal 3Shear, the results of Flournoy and Coniglio (2019) were explored as they presented a mechanism for MV development in weak line-normal shear but large wind shear *parallel* to the convective line closer to the ground—the type often present within the warm sector ahead of approaching synoptic-scale cyclones. However, there was no differentiation between MV-genesis and null line segments provided by line-parallel 1Shear; in fact, line-parallel 1Shear had a weak positive relationship to line-normal 3Shear suggesting that the mode of MV-genesis identified in Flournoy and Coniglio (2019) does not make up for the hypothesized lack of MV potential in the weak line-normal shear cases (but they still may add to the MV-genesis processes). It remains unclear why many MVs developed in relatively weak line-normal 3Shear in this study. Line-*normal* 1Shear was also examined, as cold pools may often be shallower than 3 km, but the results did not show strong discriminatory ability for MV-genesis segments compared to null segments. One potentially useful result is that all but one MV-genesis segment occurred with positive line-normal 0–1-km shear.

Regarding the relationship between the U-to-R distance and the line-normal wind shear, although the best relationship was found for wind shear in deeper layers (i.e., 0–6 km), the overall assessment of the results is that only weak-to-moderate linear correlations are seen for all shear depths (0–1, 0–3, and 0–6 km) and convective-line reflectivity thresholds tested. A reason why all line-normal shear depths showed some linear relationship to the U-to-R distance may be that cold pools likely vary substantially in depth and strength across the cases. It is likely that QLCS cold pools in the central United States (Bryan et al. 2005; Engerer et al. 2008) are typically stronger and deeper than those in the southeast United States (McDonald and Weiss 2021). Applying an approximation of 3 km to match all cold pools therefore appears suspect across a wide continuum of geographic and seasonally disparate QLCS events. While this study does not address ways to assess cold pool depth in operational settings (assessing surface pressure deficits is one potential useful proxy; Engerer et al. 2008), assessing wind shear within the 3-km depth ascribed

by the 3IM may prove unreliable as a one size fits all approach to determine the shear needed for a favorable balance regime.

Contrary to the shortfalls identified in the assessment of line-normal 3Shear, it is encouraging that most MVs occurred within a relatively small range of U-to-R distances. While a wide variety of UDCZ-to-reflectivity distances existed across study cases and analysis segments, a distance range from −5 to 5 km was observed for almost all MV-genesis events identified. This finding offers the potential to better quantify the first ingredient in the 3IM approach using an objective criterion that can be readily applied in operational settings. Also, encouraging is the existence of MV-genesis events exhibiting similar measures of the U-to-R distance, despite varying magnitudes of line-normal 0–3-km wind shear (8 kt in Fig. 23a versus 39 kt in Fig. 23b).

Additionally, the frequent occurrence of rear-inflow surges associated with MVs in this dataset confirms the appropriateness of ingredient 3. Once again, the ability to readily identify these features through radar analysis provides an opportunity to immediately apply this finding in operational settings. While the radar analysis conducted to identify surges was subjective in nature, operational guidance that applies similar methodology currently exists to identify these features in warning-decision settings (LaDue and Przybylinski 2010).

Through the analysis conducted above, we have identified *possible* guidelines to help identify convective environments *unlikely* to support persistent MV genesis. In summary, persistent QLCS MVs appear to be *unlikely* when

- updrafts are more than 5 km ahead of or behind the UDCZ;
- there are <0 kt of 0–1-km, <10 kt of 0–3-km, and <20 kt of 0–6-km line-normal wind shear; and
- no rear-inflow surge or bowing structure is present or appears imminent along the leading convective line.

We recognize that the guidelines above introduce a wide range of line-normal shear magnitudes for which MVs are considered possible. However, this accurately reflects observed environments over a geographically and seasonally disparate set of observed QLCS events. In fact, applying the lower bound (discriminatory) magnitude of 0–3-km line-normal wind shear shows improved POD (with nominal increase/decrease to FAR/CSI) when compared to the original 3IM threshold value among cases in our dataset (Tables 1 and 2). Similar performance measures are also captured when applying the 0–6-km line-normal wind shear magnitude above (Table 3). However, with a decreasing true skill statistic (TSS) (Tables 1–3) for the lower bound 0–3-km line-normal shear, *the above guidelines more accurately serve as a means to enhance forecaster situational awareness rather than strict "rules" during QLCS warning operations.*

Although this study used a relatively large dataset of observed QLCS cases/events, tested for internal characteristics at relatively small intervals (i.e., 15 km), and used observed proximity soundings in the inflow of QLCSs, a few caveats deserve additional discussion. The most important of these is the use of proximity sounding data to quantify the background environment that may undergo rapid modification (King et al. 2017). Rapid
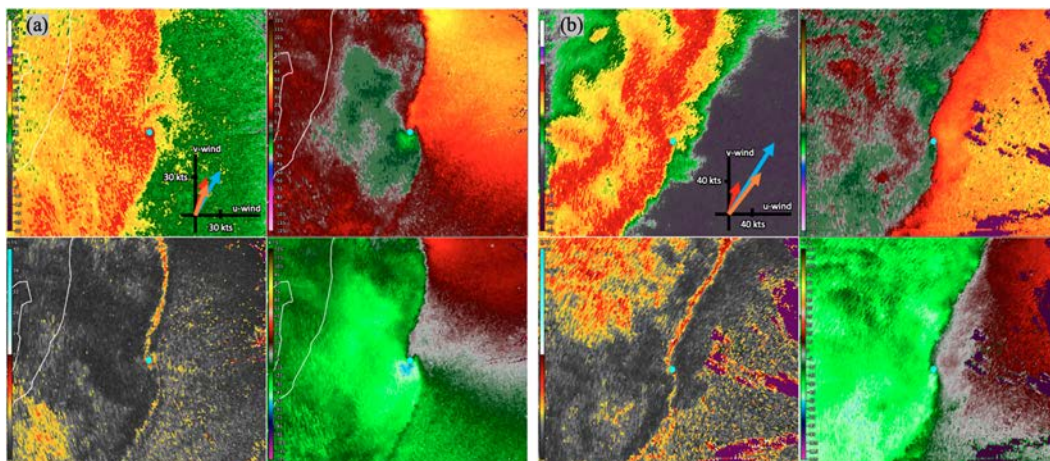
FIG. 23. (a) Multipanel display of single and dual-polarimetric radar variables from an MV-genesis event, in a regime with <30 kt of (line-normal) 0–3-km wind shear, on 28 Aug 2018 across northern Michigan. Variables (and respective panel position) are as in Fig. 7. Image from KAPX (at 0.5° elevation) valid at 2330 UTC. The cyan dot corresponds to subjectively analyzed centroid of MV. Approximate *bulk* wind shear vectors displayed in the top-left panel of (a) and (b), with the wind profile shifted so that surface wind is zero at the origin. The red arrow corresponds to 0–1-km *bulk* wind shear, orange corresponds to 0–3-km *bulk* wind shear, and light blue corresponds to 0–6-km *bulk* wind shear. (b) As in (a), but for an MV-genesis event in a regime with >30 kt of (line-normal) 0–3-km wind shear, on 11 Apr 2011 across central Alabama. Image from Birmingham, Alabama (KBMX), (at 0.5° elevation) valid at 2348 UTC.

storm-scale modifications and large heterogeneities represent a challenge in accurately capturing the "true" environment using proximity sounding data. In addition, strong mid- and upper-level winds may introduce significant horizontal displacement of certain soundings (and associated measures) from a study event of interest. As described in section 2, extra consideration was given at the onset of case selection to choose events in which the associated proximity sounding has the greatest potential to represent the true background atmosphere, but it is not possible to precisely know the extent to which this dataset represents the true ambient environment.

To continue to build operational guidance for MV-genesis identification and warning strategies, future work should focus on increasing QLCS samples with more tightened proximity criteria among all cases, along with focusing on *observed* soundings when possible given the errors in the depiction of low-level wind profiles/shear found in model analyses of environments (Taszarek et al. 2021; Coniglio and Jewell 2022). Although this study is unique in that the line orientations were defined every 15 km and approximately every 10–12 min for multiple periods within each case (identifying 1820 line segments to analyze), the overall case size here (50) limits overall robustness of the variable outcomes as is typical with most strictly observation-based analysis of environments in proximity to convection. Traditionally, field projects with mobile sounding and profiling systems have been a means to obtain samples of storm environments much faster than waiting for fortuitous NWS operational releases. However, only 9 QLCS cases with at least one usable proximity sounding from field projects were identified among the 50 cases used here. This lack of observed data near QLCSs provides significant motivation for the ongoing VORTEX-SE projects, including the recent PERiLS

TABLE 1. Contingency table comparing the 3IM threshold value of 0–3-km wind shear against MV-genesis outcomes. Additional forecast verification statistics are also included. Assumption of U-to-R distance $-5 < x < 5$ km and surge present.

		MV-genesis event observed	
		Y	N
0–3-km wind shear > 30 kt	Y	16	102
	N	14	194
Probability of detection (POD)		0.53	
False alarm rate (FAR)		0.86	
Critical success index (CSI)		0.12	
True skill statistic (TSS)		0.18	

TABLE 2. Contingency table comparing the "discriminatory" value of 0–3-km wind shear, described in section 4, against MV-genesis outcomes. Additional forecast verification statistics are also included. Assumption of U-to-R distance $-5 < x < 5$ km and surge present.

		MV-genesis event observed	
		Y	N
0–3-km wind shear > 10 kt	Y	29	257
	N	1	39
Probability of detection (POD)		0.97	
False alarm rate (FAR)		0.90	
Critical success index (CSI)		0.10	
True skill statistic (TSS)		0.10	

TABLE 3. Contingency table comparing the "discriminatory" value of 0–6-km wind shear, described in section 4, against MV-genesis outcomes. Additional forecast verification statistics are also included. Assumption of U-to-R distance $-5 < x < 5$ km and surge present.

		MV-genesis event observed	
		Y	N
0–6-km wind shear > 20 kt	Y	29	266
	N	1	30
Probability of detection (POD)		0.97	
False alarm rate (FAR)		0.90	
Critical success index (CSI)		0.10	
True skill statistic (TSS)		0.07	

(Propagation, Evolution and Rotation in Linear Storms; Rasmussen et al. 2015) project, for which a primary motivation was to better understand the rapidity of environment evolution and the connection between QLCSs and their environments. Proximity soundings and vertical profiles of the wind (and thermodynamic) variables are being collected during these campaigns that should provide a large increase in the data available to continue exploring the robustness of the results presented here.

Data availability statement. The versions of these data used in this study can be accessed by contacting the corresponding author. Data from the field-project soundings were accessed via the Earth Observing Laboratory (EOL) (available at https://www.eol.ucar.edu/all-field-programs), and data for the National Weather Service soundings were accessed via the National Center for Environmental Information (NCEI) Integrated Global Radiosonde Archive (IGRA) version 2 (available at https://www.ncei.noaa.gov/pub/data/igra). WSR-88D data were accessed via NCEI/Amazon Cloud Database (available at https://s3.amazonaws.com/noaa-nexrad-level2/index.html). All of the data analyzed for this study and further information about data processing are available upon request from the National Severe Storms Laboratory through the second author (Michael.Coniglio@noaa.gov).

REFERENCES

Alfaro, D. A., 2017: Low-tropospheric shear in the structure of squall lines: Impacts on latent heating under layer-lifting ascent. *J. Atmos. Sci.*, **74**, 229–248, https://doi.org/10.1175/JAS-D-16-0168.1.

——, and F. Lezana, 2022: A momentum-balance theory for the updraft structure in density currents analogous to squall lines. *Atmósfera*, **35**, 197–220, https://doi.org/10.20937/ATM.52899.

Ashley, W. S., A. M. Haberlie, and J. Strohm, 2019: A climatology of quasi-linear convective systems and their hazards in the United States. *Wea. Forecasting*, **34**, 1605–1631, https://doi.org/10.1175/WAF-D-19-0014.1.

Atkins, N. T., and M. St. Laurent, 2009a: Bow echo mesovortices. Part I: Processes that influence their damaging potential. *Mon. Wea. Rev.*, **137**, 1497–1513, https://doi.org/10.1175/2008MWR2649.1.

——, and ——, 2009b: Bow echo mesovortices. Part II: Their genesis. *Mon. Wea. Rev.*, **137**, 1514–1532, https://doi.org/10.1175/2008MWR2650.1.

——, J. M. Arnott, R. W. Przybylinski, R. A. Wolf, and B. D. Ketcham, 2004: Vortex structure and evolution within bow echoes. Part I: Single-Doppler and damage analysis of the 29 June 1998 derecho. *Mon. Wea. Rev.*, **132**, 2224–2242, https://doi.org/10.1175/1520-0493(2004)132<2224:VSAEWB>2.0.CO;2.

——, C. S. Bouchard, R. W. Przybylinski, R. J. Trapp, and G. Schmocker, 2005: Damaging surface wind mechanisms within the 10 June 2003 Saint Louis bow echo during BAMEX. *Mon. Wea. Rev.*, **133**, 2275–2296, https://doi.org/10.1175/MWR2973.1.

Brotzge, J. A., S. E. Nelson, R. L. Thompson, and B. T. Smith, 2013: Tornado probability of detection and lead time as a function of convective mode and environmental parameters. *Wea. Forecasting*, **28**, 1261–1276, https://doi.org/10.1175/WAF-D-12-00119.1.

Bryan, G. H., and R. Rotunno, 2014: The optimal state for gravity currents in shear. *J. Atmos. Sci.*, **71**, 448–468, https://doi.org/10.1175/JAS-D-13-0156.1.

——, D. Ahijevych, C. Davis, S. Trier, and M. Weisman, 2005: Observations of cold pool properties in mesoscale convective systems during BAMEX. Preprints, *11th Conf. on Mesoscale Processes*, Albuquerque, NM, Amer. Meteor. Soc., JP5J.12, http://ams.confex.com/ams/pdfpapers/96718.pdf.

——, J. C. Knievel, and M. D. Parker, 2006: A multimodel assessment of RKW theory's relevance to squall-line characteristics. *Mon. Wea. Rev.*, **134**, 2772–2792, https://doi.org/10.1175/MWR3226.1.

Carbone, R. E., 1982: A severe frontal rainband. Part I: Storm-wide hydrodynamic structure. *J. Atmos. Sci.*, **39**, 258–279, https://doi.org/10.1175/1520-0469(1982)039<0258:ASFRPI>2.0.CO;2.

——, 1983: A severe frontal rainband. Part II: Tornado parent vortex circulation. *J. Atmos. Sci.*, **40**, 2639–2654, https://doi.org/10.1175/1520-0469(1983)040<2639:ASFRPI>2.0.CO;2.

Cohen, A. E., M. C. Coniglio, S. F. Corfidi, and S. J. Corfidi, 2007: Discrimination of mesoscale convective system environments using sounding observations. *Wea. Forecasting*, **22**, 1045–1062, https://doi.org/10.1175/WAF1040.1.

Coniglio, M. C., and R. E. Jewell, 2022: SPC mesoscale analysis compared to field-project soundings: Implications for supercell environment studies. *Mon. Wea. Rev.*, **150**, 567–588, https://doi.org/10.1175/MWR-D-21-0222.1.

——, D. J. Stensrud, and L. J. Wicker, 2006: Effects of upper-level shear on the structure and maintenance of strong quasi-linear mesoscale convective systems. *J. Atmos. Sci.*, **63**, 1231–1252, https://doi.org/10.1175/JAS3681.1.

——, H. E. Brooks, S. J. Weiss, and S. F. Corfidi, 2007: Forecasting the maintenance of quasi-linear mesoscale convective systems. *Wea. Forecasting*, **22**, 556–570, https://doi.org/10.1175/WAF1006.1.

Conrad, D. M., and K. R. Knupp, 2019: Doppler radar observations of horizontal shearing instability in quasi-linear convective systems. *Mon. Wea. Rev.*, **147**, 1297–1318, https://doi.org/10.1175/MWR-D-18-0257.1.

Dial, G. L., J. P. Racy, and R. L. Thompson, 2010: Short-term convective mode evolution along synoptic boundaries. *Wea. Forecasting*, **25**, 1430–1446, https://doi.org/10.1175/2010WAF2222315.1.

Engerer, N. A., D. J. Stensrud and M. C. Coniglio, 2008: Surface characteristics of observed cold pools. *Mon. Wea. Rev.*, **136**, 4839–4849, https://doi.org/10.1175/2008MWR2528.1.

Evans, M., 2010: An examination of low CAPE/high shear severe convective events in the Binghamton, New York county warning area. *Natl. Wea. Dig.*, **34**, 129–144.

Flournoy, M. D., and M. C. Coniglio, 2019: Origins of vorticity in a simulated tornadic mesovortex observed during PECAN on 6 July 2015. *Mon. Wea. Rev.*, **147**, 107–134, https://doi.org/10.1175/MWR-D-18-0221.1.

Fovell, R. G., and P. S. Dailey, 1995: The temporal behavior of numerically simulated multicell-type storms. Part I: Modes of behavior. *J. Atmos. Sci.*, **52**, 2073–2095, https://doi.org/10.1175/1520-0469(1995)052<2073:TTBONS>2.0.CO;2.

Fujita, T. T., 1978: Manual of downburst identification for project Nimrod. Satellite and Mesometeorology Research Paper 156, Dept. of Geophysical Sciences, University of Chicago, 104 pp.

Geerts, B., and Coauthors, 2017: The 2015 Plains Elevated Convection At Night Field project. *Bull. Amer. Meteor. Soc.*, **98**, 767–786, https://doi.org/10.1175/BAMS-D-15-00257.1.

Gibbs, J. G., 2021: Evaluating precursor signals for QLCS tornado and higher impact straight-line wind events. *J. Oper. Meteor.*, **9**, 62–75, https://doi.org/10.15191/nwajom.2021.0905.

——, and B. R. Bowers, 2019: Techniques and thresholds of significance for using WSR-88D velocity data to anticipate significant tornadoes. *J. Oper. Meteor.*, **7**, 117–137, https://doi.org/10.15191/nwajom.2019.0709.

Goodnight, J. S., D. A. Chehak, and R. J. Trapp, 2022: Quantification of QLCS tornadogenesis, associated characteristics, and environments across a large sample. *Wea. Forecasting*, **37**, 2087–2105, https://doi.org/10.1175/WAF-D-22-0016.1.

Haberlie, A. M., and W. S. Ashley, 2019: A radar-based climatology of mesoscale convective systems in the United States. *J. Climate*, **32**, 1591–1606, https://doi.org/10.1175/JCLI-D-18-0559.1.

Hane, C. E., 1973: The squall line thunderstorm: Numerical experimentation. *J. Atmos. Sci.*, **30**, 1672–1690, https://doi.org/10.1175/1520-0469(1973)030<1672:TSLTNE>2.0.CO;2.

James, R. P., J. M. Fritsch, and P. M. Markowski, 2005: Environmental distinctions between cellular and slabular convective lines. *Mon. Wea. Rev.*, **133**, 2669–2691, https://doi.org/10.1175/MWR3002.1.

Jewett, B. F., and R. B. Wilhelmson, 2006: The role of forcing in cell morphology and evolution within midlatitude squall lines. *Mon. Wea. Rev.*, **134**, 3714–3734, https://doi.org/10.1175/MWR3164.1.

Jorgensen, D. P., and B. F. Smull, 1993: Mesovortex circulations seen by airborne Doppler radar within a bow-echo mesoscale convective system. *Bull. Amer. Meteor. Soc.*, **74**, 2146–2158, https://doi.org/10.1175/1520-0477(1993)074<2146:MCSBAD>2.0.CO;2.

King, J. R., M. D. Parker, K. D. Sherburn, and G. M. Lackmann, 2017: Rapid evolution of cool season, low-CAPE severe thunderstorm environments. *Wea. Forecasting*, **32**, 763–779, https://doi.org/10.1175/WAF-D-16-0141.1.

Kirkpatrick, J. C., E. W. McCaul Jr., and C. Cohen, 2007: The motion of simulated convective storms as a function of basic environmental parameters. *Mon. Wea. Rev.*, **135**, 3033–3051, https://doi.org/10.1175/MWR3447.1.

LaDue, J. G., and R. Przybylinski, 2010: QLCS storm-scale interrogation and warning considerations. AWOC Severe Track FY10, 28 pp., https://training.weather.gov/wdtd/courses/woc/documentation/severe/qlcs.pdf.

Lee, B. D., and R. B. Wilhelmson, 1997a: The numerical simulation of non-supercell tornadogenesis. Part I: Initiation and evolution of pretornadic misocyclone circulations along a dry outflow boundary. *J. Atmos. Sci.*, **54**, 32–60, https://doi.org/10.1175/1520-0469(1997)054<0032:TNSONS>2.0.CO;2.

——, and ——, 1997b: The numerical simulation of non-supercell tornadogenesis. Part II: Evolution of a family of tornadoes along a weak outflow boundary. *J. Atmos. Sci.*, **54**, 2387–2415, https://doi.org/10.1175/1520-0469(1997)054<2387:TNSONT>2.0.CO;2.

Lovell, L. T., and M. D. Parker, 2022: Simulated QLCS vortices in a high-shear, low-CAPE environment. *Wea. Forecasting*, **37**, 989–1012, https://doi.org/10.1175/WAF-D-21-0133.1.

Marion, G. R., and R. J. Trapp, 2021: Controls of quasi-linear convective system tornado intensity. *J. Atmos. Sci.*, **78**, 1189–1205, https://doi.org/10.1175/JAS-D-20-0164.1.

McDonald, J. M., and C. C. Weiss, 2021: Cold pool characteristics of tornadic quasi-linear convective systems and other convective modes observed during VORTEX-SE. *Mon. Wea. Rev.*, **149**, 821–840, https://doi.org/10.1175/MWR-D-20-0226.1.

Mulholland, J. P., J. M. Peters, and H. Morrison, 2021: How does vertical wind shear influence entrainment in squall lines? *J. Atmos. Sci.*, **78**, 1931–1946, https://doi.org/10.1175/JAS-D-20-0299.1.

Newman, J. F., and P. L. Heinselman, 2012: Evolution of a quasi-linear convective system sampled by phased array radar. *Mon. Wea. Rev.*, **140**, 3467–3486, https://doi.org/10.1175/MWR-D-12-00003.1.

Parker, M. D., 2010: Relationship between system slope and updraft intensity in squall lines. *Mon. Wea. Rev.*, **138**, 3572–3578, https://doi.org/10.1175/2010MWR3441.1.

——, and R. H. Johnson, 2004: Simulated convective lines with leading precipitation. Part I: Governing dynamics. *J. Atmos. Sci.*, **61**, 1637–1655, https://doi.org/10.1175/1520-0469(2004)061<1637:SCLWLP>2.0.CO;2.

Przybylinski, R. W., 1995: The bow echo: Observations, numerical simulations, and severe weather detection methods. *Wea. Forecasting*, **10**, 203–218, https://doi.org/10.1175/1520-0434(1995)010<0203:TBEONS>2.0.CO;2.

Rasmussen, E., and Coauthors, 2015: VORTEX-Southeast program overview. National Severe Storms Laboratory Rep., 36 pp.

Rotunno, R., J. B. Klemp, and M. L. Weisman, 1988: A theory for strong, long-lived squall lines. *J. Atmos. Sci.*, **45**, 463–485, https://doi.org/10.1175/1520-0469(1988)045<0463:ATFSLL>2.0.CO;2.

Schaumann, J. S., and J. Gagan, 2018: Three ingredients method. Warning Decision Training Division, 1 pp., https://training.weather.gov/wdtd/courses/woc/documentation/severe/three-ingredients-timebudget.pdf.

——, and R. W. Przybylinski, 2012: Operational application of 0–3 km bulk shear vectors in assessing quasi linear convective system mesovortex and tornado potential. *26th Conf. on Severe Local Storms*, Nashville, TN, Amer. Meteor. Soc., 142, https://ams.confex.com/ams/26SLS/webprogram/Paper212008.html.

Schenkman, A. D., M. Xue, and A. Shapiro, 2012: Tornadogenesis in a simulated mesovortex within a mesoscale convective system. *J. Atmos. Sci.*, **69**, 3372–3390, https://doi.org/10.1175/JAS-D-12-038.1.

——, ——, and M. Hu, 2014: Tornadogenesis in a high-resolution simulation of the 8 May 2003 Oklahoma City supercell. *J. Atmos. Sci.*, **71**, 130–154, https://doi.org/10.1175/JAS-D-13-073.1.

Sessa, M. F., and R. J. Trapp, 2020: Observed relationship between tornado intensity and pretornadic mesocyclone characteristics. *Wea. Forecasting*, **35**, 1243–1261, https://doi.org/10.1175/WAF-D-19-0099.1.

Shapiro, A., 1992: A hydrodynamical model of shear flow over semi-infinite barriers with application to density currents. *J. Atmos. Sci.*, **49**, 2293–2305, https://doi.org/10.1175/1520-0469(1992)049<2293:AHMOSF>2.0.CO;2.

Sherburn, K. D., and M. D. Parker, 2014: Climatology and ingredients of significant severe convection in high-shear, low-CAPE environments. *Wea. Forecasting*, **29**, 854–877, https://doi.org/10.1175/WAF-D-13-00041.1.

Smith, B. T., R. L. Thompson, J. S. Grams, C. Broyles, and H. E. Brooks, 2012: Convective modes for significant severe thunderstorms in the contiguous United States. Part I: Storm classification and climatology. *Wea. Forecasting*, **27**, 1114–1135, https://doi.org/10.1175/WAF-D-11-00115.1.

——, ——, A. R. Dean, and P. T. Marsh, 2015: Diagnosing the conditional probability of tornado damage rating using environmental and radar attributes. *Wea. Forecasting*, **30**, 914–932, https://doi.org/10.1175/WAF-D-14-00122.1.

Stensrud, D. J., M. C. Coniglio, R. P. Davies-Jones, and J. S. Evans, 2005: Comments on "'A theory for strong long-lived squall lines' revisited." *J. Atmos. Sci.*, **62**, 2989–2996, https://doi.org/10.1175/JAS3514.1.

Szeto, K. K., and H.-R. Cho, 1994: A numerical investigation of squall lines. Part II: The mechanics of evolution. *J. Atmos. Sci.*, **51**, 425–433, https://doi.org/10.1175/1520-0469(1994)051<0425:ANIOSL>2.0.CO;2.

Taszarek, M., N. Pilguj, J. T. Allen, V. Gensini, H. E. Brooks, and P. Szuster, 2021: Comparison of convective parameters derived from ERA5 and MERRA-2 with rawinsonde data over Europe and North America. *J. Climate*, **34**, 3211–3237, https://doi.org/10.1175/JCLI-D-20-0484.1.

Thompson, R. L., R. Edwards, J. A. Hart, K. L. Elmore, and P. Markowski, 2003: Close proximity soundings within supercell environments obtained from the rapid update cycle. *Wea. Forecasting*, **18**, 1243–1261, https://doi.org/10.1175/1520-0434(2003)018<1243:CPSWSE>2.0.CO;2.

——, B. T. Smith, J. S. Grams, A. R. Dean, and C. Broyles, 2012: Convective modes for significant severe thunderstorms in the contiguous United States. Part II: Supercell and QLCS tornado environments. *Wea. Forecasting*, **27**, 1136–1154, https://doi.org/10.1175/WAF-D-11-00116.1.

Thorpe, A. J., M. J. Miller, and M. W. Moncrieff, 1982: Two-dimensional convection in non-constant shear: A model of mid-latitude squall lines. *Quart. J. Roy. Meteor. Soc.*, **108**, 739–762, https://doi.org/10.1002/qj.49710845802.

Trapp, R. J., and M. L. Weisman, 2003: Low-level mesovortices within squall lines and bow echoes. Part II: Their genesis and implications. *Mon. Wea. Rev.*, **131**, 2804–2823, https://doi.org/10.1175/1520-0493(2003)131<2804:LMWSLA>2.0.CO;2.

——, S. A. Tessendorf, E. S. Godfrey, and H. E. Brooks, 2005: Tornadoes from squall lines and bow echoes. Part I: Climatological distribution. *Wea. Forecasting*, **20**, 23–34, https://doi.org/10.1175/WAF-835.1.

van den Broeke, M. S., D. M. Schultz, R. H. Johns, J. S. Evans, and J. E. Hales, 2005: Cloud-to-ground lightning production in strongly forced, low-instability convective lines associated with damaging wind. *Wea. Forecasting*, **20**, 517–530, https://doi.org/10.1175/WAF876.1.

Wakimoto, R. M., H. V. Murphey, C. A. Davis, and N. T. Atkins, 2006: High winds generated by bow echoes. Part II: The relationship between the mesovortices and damaging straight-line winds. *Mon. Wea. Rev.*, **134**, 2813–2829, https://doi.org/10.1175/MWR3216.1.

——, P. Stauffer, and W.-C. Lee, 2015: The vertical vorticity structure within a squall line observed during BAMEX: Banded vorticity features and the evolution of a bowing segment. *Mon. Wea. Rev.*, **143**, 341–362, https://doi.org/10.1175/MWR-D-14-00246.1.

Weisman, M. L., 1992: The role of convectively generated rear-inflow jets in the evolution of long-lived mesoconvective systems. *J. Atmos. Sci.*, **49**, 1826–1847, https://doi.org/10.1175/1520-0469(1992)049<1826:TROCGR>2.0.CO;2.

——, and R. J. Trapp, 2003: Low-level mesovortices within squall lines and bow echoes. Part I: Overview and dependence on environmental shear. *Mon. Wea. Rev.*, **131**, 2779–2803, https://doi.org/10.1175/1520-0493(2003)131<2779:LMWSLA>2.0.CO;2.

——, and R. Rotunno, 2004: "A theory for strong long-lived squall lines" revisited. *J. Atmos. Sci.*, **61**, 361–382, https://doi.org/10.1175/1520-0469(2004)061<0361:ATFSLS>2.0.CO;2.

——, J. B. Klemp, and R. Rotunno, 1988: Structure and evolution of numerically simulated squall lines. *J. Atmos. Sci.*, **45**, 1990–2013, https://doi.org/10.1175/1520-0469(1988)045<1990:SAEONS>2.0.CO;2.

Wheatley, D. M., and R. J. Trapp, 2008: The effect of mesoscale heterogeneity on the genesis and structure of mesovortices within quasi-linear convective systems. *Mon. Wea. Rev.*, **136**, 4220–4241, https://doi.org/10.1175/2008MWR2294.1.

——, ——, and N. T. Atkins, 2006: Radar and damage analysis of severe bow echoes observed during BAMEX. *Mon. Wea. Rev.*, **134**, 791–806, https://doi.org/10.1175/MWR3100.1.

Xu, X., M. Xue, and Y. Wang, 2015: The genesis of mesovortices within a real-data simulation of a bow echo system. *J. Atmos. Sci.*, **72**, 1963–1986, https://doi.org/10.1175/JAS-D-14-0209.1.

Xu, Q., and M. W. Moncrieff, 1994: Density current circulations in shear flows. *J. Atmos. Sci.*, **51**, 434–446, https://doi.org/10.1175/1520-0469(1994)051<0434:DCCISF>2.0.CO;2.